PACIFIC EARTHQUAKE ENGINEERING
RESEARCH CENTER

A Beam-Column Joint Model for Simulating the Earthquake Response of Reinforced Concrete Frames

Laura N. Lowes
Nilanjan Mitra
University of Washington

and

Arash Altoontash
Stanford University

PEER 2003/10
FEB. 2004

A Beam-Column Joint Model for Simulating the Earthquake Response of Reinforced Concrete Frames

Laura N. Lowes
University of Washington

Nilanjan Mitra
University of Washington

Arash Altoontash
Stanford University

PEER Report 2003/10
Pacific Earthquake Engineering Research Center
College of Engineering
University of California, Berkeley
February 2004

ABSTRACT

Experimental investigation of the earthquake response of reinforced concrete subassemblages indicates that stiffness and strength loss resulting from beam-column joint damage may be substantial. To simulate inelastic joint action, a joint element is developed that is appropriate for use with traditional beam-column elements in two-dimensional nonlinear frame analysis. The proposed element formulation includes four external nodes with a total of 12 external degrees of freedom; however, the element is a super-element and includes four additional internal degrees of freedom. The super-element comprises 13 one-dimensional components that explicitly represent the three types of inelastic mechanisms that may determine the earthquake response of beam-column joints: anchorage failure of beam and column longitudinal reinforcement embedded in the joint, shear failure of the joint core, and shear-transfer failure at the beam-joint and column-joint interfaces. Calibration models are proposed for each of the three types of components. These calibration models enable a user to predict response as a function of concrete compressive strength, transverse steel ratio, frame-member longitudinal steel properties, and joint geometry. Comparison of simulated and observed response for subassemblages tested in the laboratory indicates that the proposed model is appropriate for use in simulating the earthquake response of building joints with moderate earthquake load demands.

ACKNOWLEDGMENTS

This work was supported in part by the Pacific Earthquake Engineering Research Center through the Earthquake Engineering Research Centers Program of the National Science Foundation under award number EEC-9701568.

CONTENTS

LIST OF FIGURES

LIST OF TABLES

1 Introduction

Typically, in modeling the response of reinforced concrete structures to earthquake loading, it is assumed that inelastic action is limited to flexural yielding of beams, columns, slabs and walls. However, experimental data [Walker 2001; Mazzoni and Moehle 2001; Clyde et al. 2000; Lowes and Moehle 1999; Leon 1990; Meinheit and Jirsa 1977; Park and Ruitong 1988; Durrani and Wight 1985] suggest that numerical simulation of both newly designed and existing structures requires representation of the inelastic response of beam-column joints. Here, a simple beam-column joint element is proposed that enables simulation of the primary mechanisms that determine the inelastic response of joints under earthquake loading. This element is appropriate for use in two-dimensional analysis with traditional hysteretic beam-column line elements to predict the response of reinforced concrete frames. The proposed element may be calibrated to simulate the response of as-built and newly designed joints. Calibration procedures for newly designed beam-column building joints are proposed and evaluated through comparison of simulated and observed response.

1.1 OBJECTIVES

The primary objective of the research effort presented here is the development and implementation in OpenSees (**http://opensees.peer.berkeley.edu**) of a joint model that is appropriate for use in two-dimensional frame analysis to predict the inelastic response of reinforced concrete joints under earthquake loading. It is desirable that the proposed joint model have the following characteristics:

1. Compatibility with traditional beam-column line elements: The proposed joint model should be appropriate for use with traditional beam-column line elements for two-dimensional nonlinear pseudo-static and dynamic analysis of reinforced concrete frame structures.

2. Computational efficiency: The proposed model should not increase greatly the computational effort required to accomplish two-dimensional analysis of a reinforced-concrete frame.
3. Transparency: The proposed model should represent the primary mechanisms that determine the inelastic response of beam-column joints, enabling a user to vary model parameters to investigate the impact on frame response of changes in mechanism response.
4. Objectivity in model calibration: The end user should not be required to specify arbitrary calibration parameters to predict the response of a joint with particular design details.
5. Robustness: The internal element solution algorithms should be sufficiently robust that element convergence is achieved for a broad range of plausible calibration parameters.

1.2 ORGANIZATION OF THE REPORT

This research report is organized into seven chapters. Following the introduction, Chapter 2 provides a brief review of previous research to develop beam-column joints models; the results of this research form a basis for the current research and were used to develop the research objectives presented above. Chapter 3 presents the proposed beam-column joint element formulation as well as details of the OpenSees implementation. Chapter 4 presents a general one-dimensional material model that is used to simulate the response of joint mechanisms as well as the OpenSees implementation of this model. Chapter 5 presents the proposed joint model calibration procedures that enable a user to predict the response of a beam-column joint with unique design details. Chapter 6 provides a comparison of beam-column joint subassemblage response observed in the laboratory and simulated using the proposed model.

2 Literature Review

Previous research provides several approaches to modeling beam-column joint response and using experimental data to calibrate these models. These methods range in sophistication from the use of experimental data to define moment-rotation relationships to high-resolution finite element modeling. However, these previously proposed methods do not meet the needs of the current study in terms of accuracy in simulating response, generality in model application, objectivity in model calibration, transparency in linking observed response mechanisms to the model formulation and calibration, and flexibility in modifying the model.

2.1 MODELING INELASTIC JOINT ACTION WITHIN THE BEAM-COLUMN ELEMENT

Some of the earliest work to simulate the inelastic response of reinforced concrete frames relied on the calibration of the "plastic-hinges" within beam-column line elements to introduce the inelastic action of the beam-column joint. Otani [1974] and Anderson and Townsend [1977] used response. However, a primary objective of the current study is the development of an independent joint model that can be used with multiple beam-column line-element formulations. Additionally, while this approach is computationally efficient, objective calibration of these models is extremely difficult, as is the use of these models to investigate the impact of joint design parameters on local and global response.

2.2 ROTATIONAL HINGE MODELS

The next generation of beam-column joint models decoupled the inelastic response of the beams, columns, and joints to facilitate model calibration. One such model is the zero-length rotational spring element that has been used by several researchers [El-Metwally and Chen 1988; Alath and Kunnath 1995] to connect beam elements to column elements and thereby represent the shear distortion of the beam-column joint. Typically, joint moment-rotation data from beam-column

subassemblage tests are used to calibrate this type of joint model. Alath and Kunnath, for example, recommend this approach. El-Metwally and Chen, using the assumptions that (1) anchorage failure for longitudinal reinforcement embedded in the joint controls inelastic joint action under earthquake loading and (2) total energy dissipation due to anchorage failure is approximately constant for all beam-column joints, develop a method for predicting inelastic joint moment-rotation response under cyclic loading.

While the rotational-hinge joint model provides a means of independently characterizing inelastic joint action with only a moderate increase in computational effort, this approach does not facilitate the development of objective and accurate calibration procedures. This approach requires that data from experimental testing of beam-column joint subassemblages be used to develop a one-dimensional joint moment-rotation relationship (or, for the El-Metwally and Chen model, define the maximum energy that can be dissipated through anchorage failure). Developing such a model that can be used to predict the response of joints with different design details requires either a large number of data sets and a sophisticated calibration procedure or multiple models for joints with different design details. Currently, there are not sufficient data in the literature to support the development of models that are appropriate for a broad range of joint designs.

2.3 CONTINUUM MODELS

More recently, researchers have begun using continuum-type elements to represent the response of reinforced concrete beam-column joints. In these models a “transition element” or “transition zone” is formulated to establish compatibility between beam-column line elements that represent the structure outside the joint and planar continuum elements that represent the structure inside the joint. This type of formulation greatly increases the computational effort of the analysis but offers the potential for high-resolution, accurate, and objective modeling of the joint region. To date these formulations have included extremely simple idealizations of the beam-column joint region [Fleury et al. 2000; Elmorsi et al. 2000].

This approach is not appropriate for the current study for several reasons. First, this approach adds substantial additional computational effort to an analysis, making two-dimensional dynamic analysis too time consuming for use by practicing engineers and most researchers. Second, it is unlikely that this type of model could meet the requirements for robustness under a wide range of joint designs and model parameters. Third, a continuum model

requires a user to introduce many material constitutive parameters. While most of these parameters will represent fundamental material properties, some will undoubtedly require the user to make some assumptions about material response. The impact of these assumptions on the simulation of the joint response mechanisms will typically be unclear and will often require a parameter study to verify.

2.4 SUMMARY

A variety of beam-column joint models have been proposed by other researchers. Of these models, the rotational-hinge model used by El-Metwally and Chen [1988] and Alath and Kunnath [1995] comes closest to meeting the objectives of the current study, as it provides computational efficiency, robustness, and compatibility with traditional structural analysis models. However, this model requires that a single moment-rotation relation be developed to define the inelastic response of a beam-column joint under cyclic loading, and this requirement does not facilitate the development of objective and transparent calibration procedures that are generally applicable.

3 Joint Element Formulation

The results of previous research indicate the primary mechanisms that determine the earthquake response of beam-column joints. These mechanisms, which include (1) anchorage failure of frame-member longitudinal reinforcement embedded in the joint, (2) inelastic shear response of the reinforced concrete joint core, and (3) shear-transfer failure at the joint-column and joint-beam interfaces, are represented explicitly in the proposed joint element. This element has the following characteristics:

1. The element is two-dimensional with a finite-area.
2. The element includes four external nodes with a total of 12 external degrees of freedom.
3. The element includes four internal degrees of freedoms.
4. The element includes one shear-panel component, eight bar-slip components, and four interface-shear components. All of these components have independent load-deformation response histories.

3.1 THE EARTHQUAKE RESPONSE OF BEAM-COLUMN JOINTS

Figure 3.1 shows a building subassemblage under moderate to severe earthquake loading. Typically, under this load distribution, beams develop nominal flexural strength at the joint perimeter and column longitudinal reinforcement carries tensile stress that approaches the yield stress. Figure 3.2 shows an idealization of the force distribution at the perimeter of a typical joint under earthquake loading of the building frames. Beam and column moments are assumed to transfer into the joint through tension force resultants carried by the frame-member longitudinal reinforcing steel (white arrows in Fig. 3.2) and compression force resultants carried by frame-member concrete (dark grey arrows in Fig. 3.2). Shear forces are assumed to transfer into the joint through concrete in the vicinity of the frame-member flexural compression zones (hatched arrows in Fig. 3.2). Figure 3.3 shows an idealization of the loads acting on the joint core.

Compression and shear forces are assumed to act directly on the perimeter of the joint core (dark grey and hatched arrows in Fig. 3.3), while tension forces carried in frame-member reinforcing steel are assumed to transfer into the joint core through distributed bond forces (light grey arrows in Fig. 3.3).

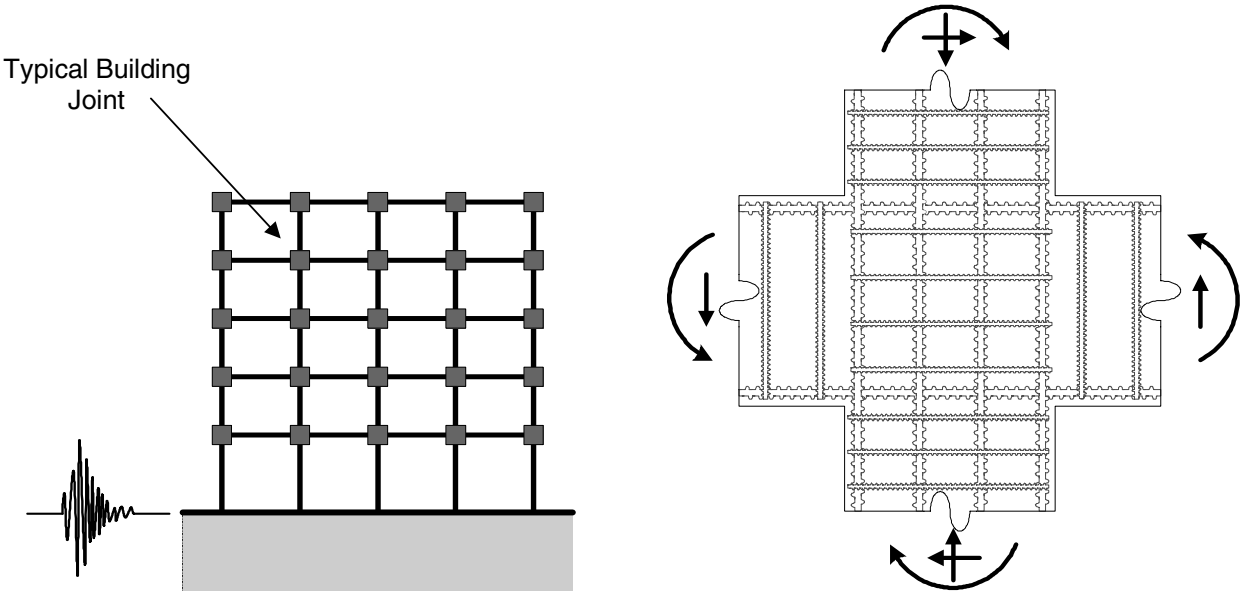

(a) Building frame under earthquake loading (b) Earthquake loading of a typical joint

Fig. 3.1. Beam-column joint loads under earthquake loading of a building frame

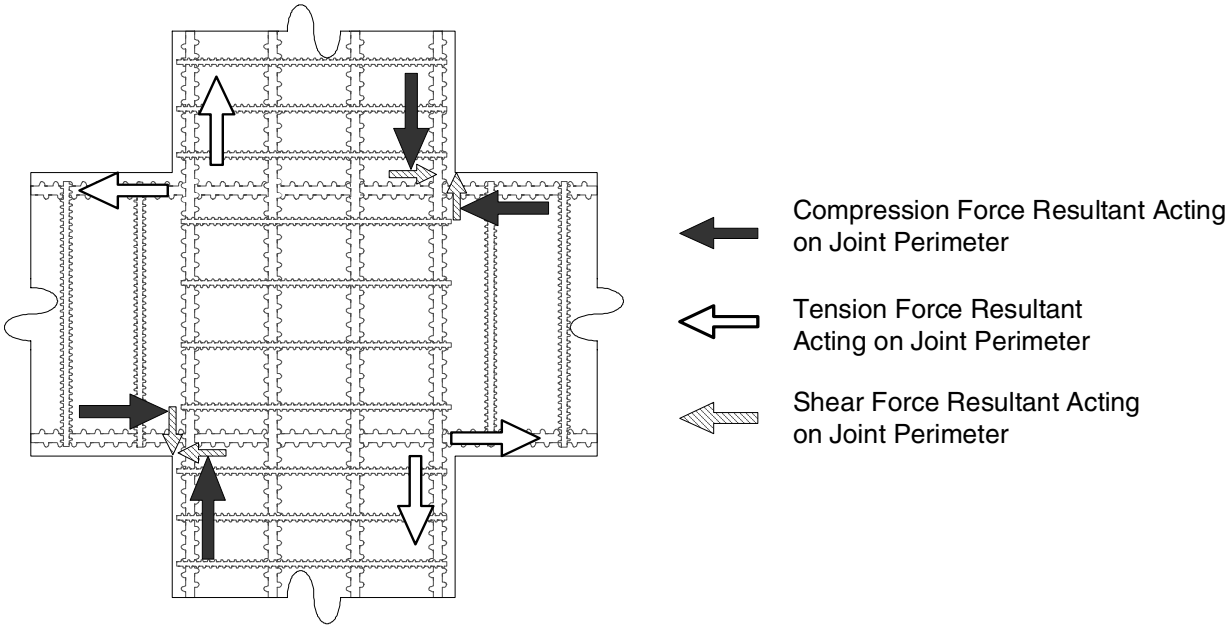

Fig. 3.2. Idealized load distribution at the perimeter of the joint

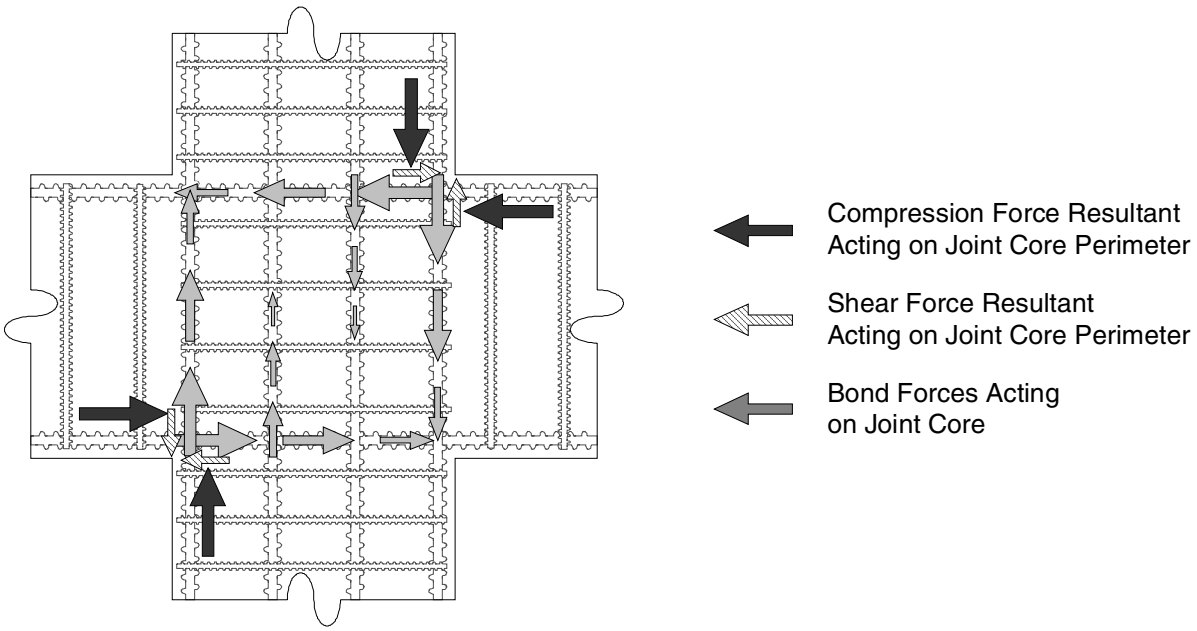

Fig. 3.3. Idealized loading of the joint core

Evaluation of the joint-core load distribution shown in Figure 3.3 provides insight into the mechanisms that determine joint response. First, the load distribution here suggests that the anchorage of longitudinal reinforcement may determine joint response. The bond-force distribution determines, in part, the total load transferred into the joint; thus, joint capacity is a function of bond strength. A review by Bonacci and Pantazopoulou [1993] of 86 interior beam-column building joint subassemblages tested in the laboratory under reversed-cyclic loading found that for 19 specimens, anchorage failure contributed to joint failure. Beyond controlling joint strength, Paulay et al. [1978] suggest that the distribution of bond stress also affects beam-column joint load-deformation response. Paulay et al. propose two equilibrium-based models of the joint; one follows from the assumption of uniform bond stress within the joint, the other requires that bond be significant only in the vicinity of the beam and column flexural compression zones. Paulay et al. suggest that these bond stress distributions are associated with different damage states and thus different deformation states of the beam-column joint.

The load distribution shown in Figure 3.3 suggests also that shear loading of the joint-core concrete may determine response. The light grey arrows indicate shear load applied to the joint core through bond. Compression stress carried in concrete at the perimeter of the joint (black compression-resultant arrows in Fig. 3.3 constitute load carried by concrete and reinforcing steel) contributes also to shear loading of the joint core. Thus, the shear strength of the joint core as well as the inelastic deformation of the joint core under the applied shear load

may determine joint response. In their review of beam-column joint tests, Bonacci and Pantazopoulou [1993] found 51 of 86 subassemblages for which failure was determined, in part, by joint shear failure. Paulay et al. [1978] identify two different load distributions within the joint core that represent the extremes of shear-load transfer within the joint. One load-distribution follows from the assumption that the reinforced concrete joint core carries essentially uniform shear stress; damage is assumed also to be relatively well distributed and uniform. A second load-distribution follows from the assumption that load is transferred primarily through compression of the joint-core concrete; damage results from dilation of the compression zone. The idealization shown in Figure 3.3 suggests that both of these shear-transfer mechanisms may be active.

In addition to the anchorage and shear response mechanisms, the proposed model includes also an interface-shear component to represent increased sliding shear flexibility and reduced sliding shear strength at the perimeter of the joint. Experimental testing of reinforced concrete subassemblages indicates that under severe reversed-cyclic loading, concrete cracks open at the perimeter of the joint and remain open during load reversal [Ma et al. 1976]. The opening of concrete cracks reduces the strength and stiffness of interface-shear mechanisms.

3.2 THE PROPOSED JOINT MODEL

Figure 3.4 shows the proposed two-dimensional idealization of an interior beam-column building joint. This model includes eight bar-slip components that are intended to simulate stiffness and strength loss associated with bond-strength deterioration for beam and column longitudinal reinforcement embedded in the joint core, one shear-panel component that is intended to simulate strength and stiffness loss associated with shear failure of the joint core, and four interface-shear components that are intended to simulate loss of shear-transfer capacity at the joint-beam and joint-column perimeter under severe loading of the joint.

In Figure 3.4, and all other figures depicting the joint model, the bar-slip and interface-shear springs are given a finite length to facilitate discussion; however, the model is implemented with the interior and exterior planes coincident.

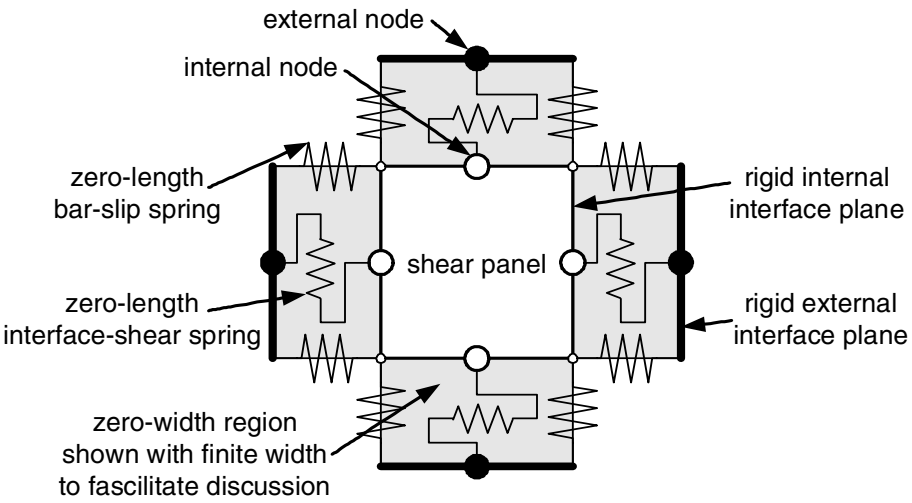

Fig. 3.4. Components of the beam-column joint model

3.3 THE ELEMENT FORMULATION

The beam-column joint model shown in Figure 3.4 is incorporated into a four-node element for use in two-dimensional modeling of building frames. This element formulation is appropriate for use in a displacement-based incrementally advancing global solution algorithm in which, for each load increment, two translational displacements and one rotation are computed at each global-model node (external nodes in Fig. 3.4) to satisfy equilibrium. It is assumed that use of the element in a global analysis requires that for a given set of imposed generalized nodal displacements, the element formulation defines a vector of generalized nodal forces representing the reactions required to develop these displacements and an element tangent matrix representing the instantaneous derivative of these forces with respect to the nodal displacements.

Unlike the typical displacement-based element formulation in which the displacement of the external nodes defines uniquely the element deformation state, the deformation state of the beam-column joint element is defined by the displacement of the external nodes and the four internal nodes (Fig. 3.5). These internal nodes are unique to the beam-column joint element, and the displacement of these nodes must be computed to satisfy internal equilibrium of the element. Thus, each iteration of the global solution algorithm requires an iterative solution of the element to determine the element state. With external and internal nodal displacements known, the nodal-force vector is computed directly from internal component forces. The element tangent matrix

used in analysis of the global structural system is computed directly from the local element tangent matrix through static condensation of the zero-value internal nodal resultants.

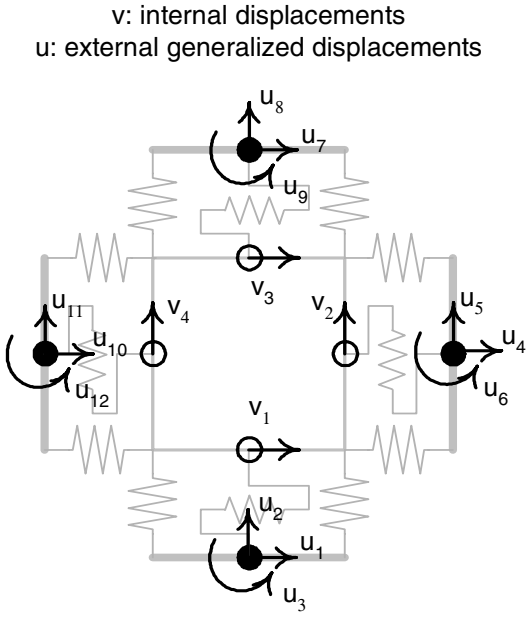

Fig. 3.5. Internal and external displacements and rotations

3.3.1 Definition of Internal Deformations and Component Loads

The material state of the beam-column joint element is defined uniquely by the displacement history of the four external and four internal element nodes. These displacement histories define the deformation history of the 12 uniaxial spring components and the single two-dimensional shear-panel component that compose the beam-column joint model. The shear-panel component is assumed to deform only in shear and, thus, to have a one-dimensional load-deformation response. Figure 3.6a shows the component deformations. Joint element component deformations are defined as a function of the external and internal nodal displacements:

$$\begin{bmatrix}\Delta_1\\ \Delta_2\\ \Delta_3\\ \Delta_4\\ \Delta_5\\ \Delta_6\\ \Delta_7\\ \Delta_8\\ \Delta_9\\ \Delta_{10}\\ \Delta_{11}\\ \Delta_{12}\\ \Delta_{13}\end{bmatrix} = \begin{bmatrix} 0 & -1 & \frac{w}{2} & 0 & 0 & 0 & 0 & 0 & 0 & 0 & 0 & 0 & 0 & 0 & 0 & 1\\ 0 & -1 & -\frac{w}{2} & 0 & 0 & 0 & 0 & 0 & 0 & 0 & 0 & 0 & 0 & 1 & 0 & 0\\ 1 & 0 & 0 & 0 & 0 & 0 & 0 & 0 & 0 & 0 & 0 & 0 & -1 & 0 & 0 & 0\\ 0 & 0 & 0 & 1 & 0 & \frac{h}{2} & 0 & 0 & 0 & 0 & 0 & 0 & -1 & 0 & 0 & 0\\ 0 & 0 & 0 & 1 & 0 & -\frac{h}{2} & 0 & 0 & 0 & 0 & 0 & 0 & 0 & 0 & -1 & 0\\ 0 & 0 & 0 & 0 & 1 & 0 & 0 & 0 & 0 & 0 & 0 & 0 & 0 & -1 & 0 & 0\\ 0 & 0 & 0 & 0 & 0 & 0 & 0 & 1 & -\frac{w}{2} & 0 & 0 & 0 & 0 & 0 & 0 & -1\\ 0 & 0 & 0 & 0 & 0 & 0 & 0 & 1 & \frac{w}{2} & 0 & 0 & 0 & 0 & -1 & 0 & 0\\ 0 & 0 & 0 & 0 & 0 & 0 & 1 & 0 & 0 & 0 & 0 & 0 & 0 & 0 & -1 & 0\\ 0 & 0 & 0 & 0 & 0 & 0 & 0 & 0 & 0 & -1 & 0 & -\frac{h}{2} & 1 & 0 & 0 & 0\\ 0 & 0 & 0 & 0 & 0 & 0 & 0 & 0 & 0 & -1 & 0 & \frac{h}{2} & 0 & 0 & 1 & 0\\ 0 & 0 & 0 & 0 & 0 & 0 & 0 & 0 & 0 & 0 & 1 & 0 & 0 & 0 & 0 & -1\\ 0 & 0 & 0 & 0 & 0 & 0 & 0 & 0 & 0 & 0 & 0 & 0 & -\frac{1}{h} & \frac{1}{w} & \frac{1}{h} & -\frac{1}{w}\end{bmatrix} \cdot \begin{bmatrix}u_1\\ u_2\\ u_3\\ u_4\\ u_5\\ u_6\\ u_7\\ u_8\\ u_9\\ u_{10}\\ u_{11}\\ u_{12}\\ v_1\\ v_2\\ v_3\\ v_4\end{bmatrix} \qquad \text{(Eq. 3.1a)}$$

$$\Delta = A \cdot \begin{Bmatrix}\boldsymbol{u}\\ \boldsymbol{v}\end{Bmatrix} \qquad \text{(Eq. 3.1b)}$$

Internal spring deformations are defined as positive for spring extension and as negative for spring compression. For interface shear springs, a positive shear deformation is associated with zero internal displacement and positive external displacement. Deformation of the shear panel follows the standard definition for engineering shear strain. One-dimensional material constitutive relationships define component forces, and thus the joint element load distribution, as a function of the component deformation history. Figure 3.6b identifies the component forces. For the bar-slip and interface-shear springs, the complementary generalized forces are forces acting in the direction of the spring axis as represented in Figures 3.2–3.6 with tension defined as positive. For the shear-panel component, the complementary component force is the moment carried by the panel through shear; Figure 3.7 shows two idealizations of this component generalized force.

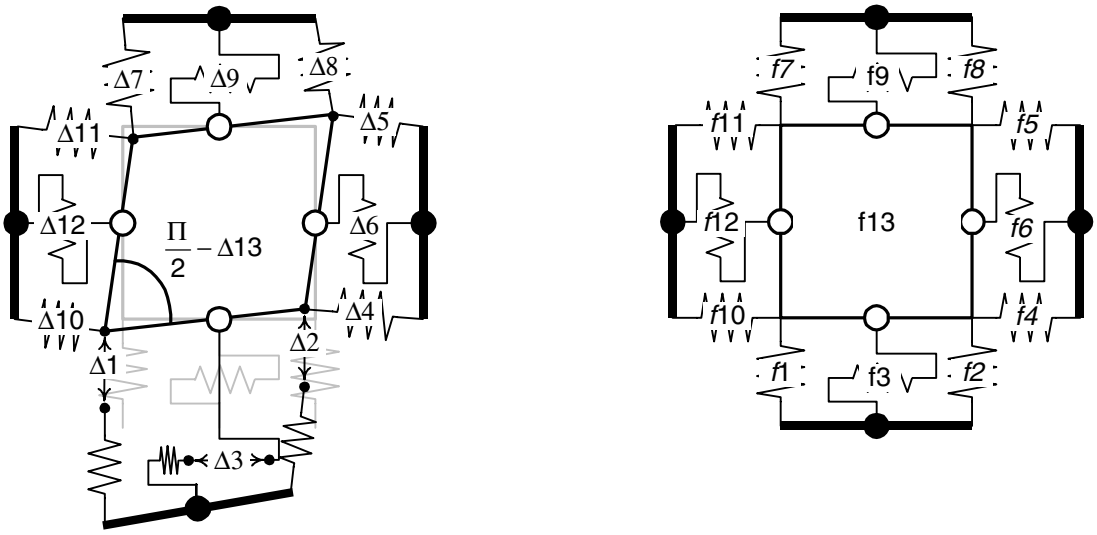

(a) Component deformations (b) Component generalized forces

Fig. 3.6. Joint element deformation and load distribution

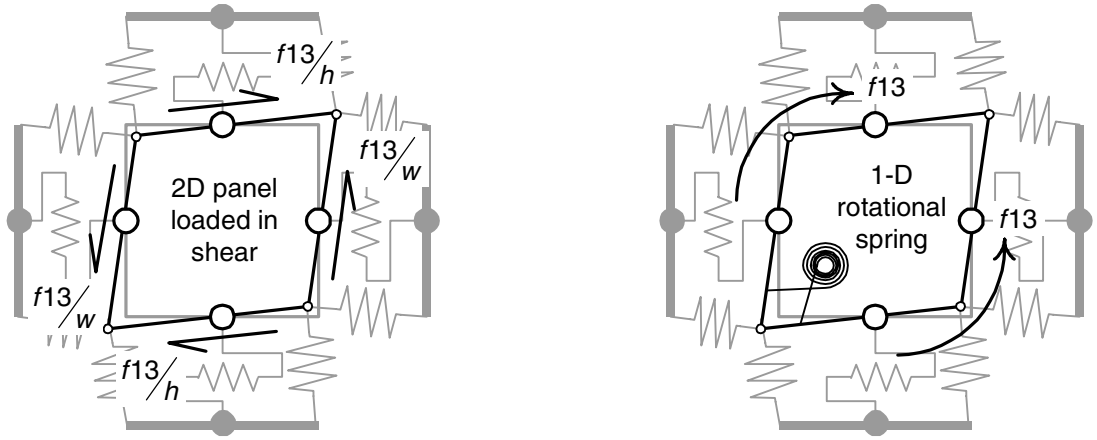

(a) Shear forces acting on the perimeter of the shear-panel component

(b) Moments acting on the shear-panel component

Fig. 3.7. Shear-panel action

Complementary to the set of 16 internal and external nodal displacements (Fig. 3.5), there is a set of 16 internal and external nodal resultants (Fig. 3.8). Nodal resultants may be computed directly from component forces by imposing equilibrium at the external and internal nodes. This results in the expected contragradient transformation between nodal resultants and component forces:

$$\begin{Bmatrix} F_1 \\ \vdots \\ F_{12} \\ \Phi_1 \\ \vdots \\ \Phi_4 \end{Bmatrix} = A^T \begin{Bmatrix} f_1 \\ \vdots \\ f_{13} \end{Bmatrix} \qquad \text{(Eq. 3.2)}$$

where F and Φ refer, respectively, to the external and internal nodal resultants defined in Figure 3.8, *f* refers to the component forces defined in Figure 3.6b, and *A* is as defined in (Eq. 3.1b. An admissible element material state includes internal nodal resultants equal to zero.

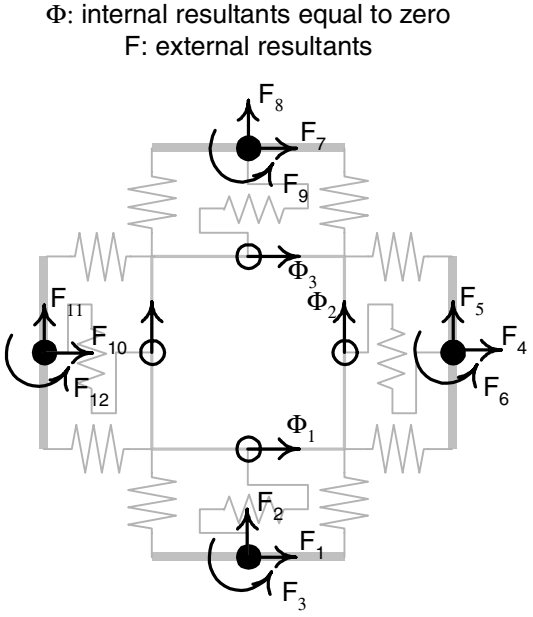

Fig. 3.8. Internal and external resultants

3.3.2 Internal Equilibrium of the Beam-Column Joint Element

Given an imposed set of external nodal displacements, determination of the element material state requires solution for the four unknown internal displacements that satisfy internal equilibrium of the element. This requires solution of four coupled nonlinear equations:

$$\begin{Bmatrix} 0 \\ 0 \\ 0 \\ 0 \end{Bmatrix} = \begin{Bmatrix} \Phi_1 \\ \Phi_2 \\ \Phi_3 \\ \Phi_4 \end{Bmatrix} = \tilde{A}^T \begin{Bmatrix} f1 \\ \vdots \\ f13 \end{Bmatrix} \qquad \text{(Eq. 3.3)}$$

where Φ and f are as defined in Equation 3.2 and $\tilde{A}$ refers to columns 10 through 13 of the transformation matrix A defined in Equation 3.1.

The solution for the internal nodal displacements, and thus the material state of the beam-column joint element, typically can be accomplished using a classical Newton-Raphson iteration scheme. The following algorithm solves for internal nodal displacements, v, at time t given the imposed external nodal displacements, u, at time t, the internal nodal displacements at the equilibrium configuration, v^{t-1}, for time $t-1$, and a set of history data defining component material response also at time $t-1$.

Joint Element Solution Algorithm

$$\Delta^0 = A \cdot \begin{Bmatrix} u \\ v^0 \end{Bmatrix} = A \cdot \begin{Bmatrix} u \\ v^{t-1} \end{Bmatrix}$$

for a = 1 to 13

  $[\kappa_a, f_a]$= *materialResponse* (Δ_a, *history*$_a$)

end

$$\Phi^0 = A^T f$$

i = 0

while $\Phi^{iT}\Phi^i > \text{tol}$

  $$v^{i+1} = v^i - \left(\tilde{A}^T k \tilde{A}\right)^{-1} \Phi^i$$

  $$\Delta^{i+1} = A \cdot \begin{Bmatrix} u \\ v^{i+1} \end{Bmatrix}$$

  for a = 1 to 13

    $[\kappa_a, f_a]$= *materialResponse* (Δ_a, *history*$_a$)

  end

  $$\Phi^{i+1} = A^T f$$

  i = i+1

end

In this algorithm, k is a diagonal matrix of the component material response tangent values, κ.

$$k_{a,a} = \kappa_a = \frac{df_a}{d\Delta_a} \qquad \text{(Eq. 3.4)}$$

Here it assumed that the material response of the components is defined by the function *materialResponse* that returns the current component force, f_a, and tangent to the force-deformation response history, κ_a, given the current component deformation, Δ_a, and a set of history data, *history*$_a$. Algorithm values $\tilde{A}$, A, and Φ are as defined previously.

The *Joint Element Solution Algorithm* will converge quadratically if the initial trial value of v is in the vicinity of the solution and if $\tilde{A}^T k \tilde{A}$ is definite. For older reinforced concrete beam-

column joints with minimal transverse reinforcement and relatively short reinforcement anchorage lengths, constitutive models defining component behavior are calibrated to describe severe stiffness and strength deterioration. For these systems, the highly nonlinear response of the joint components may result in the initial trial value of v being relatively far from the solution for a given set of external nodal displacements, u, encountered at points on the global system solution path. Further, for these beam-column joints, it is likely that the element tangent matrix $\tilde{A}^T k \tilde{A}$ may be numerically singular at some points during the internal element solution. To ensure that element convergence is achieved for any set of imposed external nodal displacement, it may be necessary to improve the robustness of the internal solution algorithm. The following modifications have been used with varying levels of success:

1. Modification of the classical Newton-Raphson solution algorithm to include a linesearch [Matthies and Strang 1979]
2. Implementation of the classical Modified Newton-Raphson solution algorithm
3. Discretization of the imposed external nodal displacement increment, to enable internal solution at discrete points along the global solution path

3.3.3 Definition of the Element Tangent and Residual

With the element state-determination complete, application of the global solution algorithm to solve for equilibrium of the structure requires computation of an element residual vector and the element stiffness matrix that defines the instantaneous derivative of the residual vector with respect to the external nodal displacements.

The element residual vector comprises the external nodal forces as defined in Figure 3.8 and is computed from internal joint component forces (Fig. 3.6b). The residual vector is defined as follows:

$$R = \{F_1 \quad F_2 \quad F_3 \quad \ldots \quad F_1 \quad F_{12}\}^T \qquad \text{(Eq. 3.5)}$$

External nodal reactions, F_1 through F_{12}, are determined by enforcing equilibrium at the joint-beam and joint-column interfaces and may be computed as follows:

$$R = \begin{Bmatrix} F_1 \\ \vdots \\ F_{12} \end{Bmatrix} = \hat{A}^T \begin{Bmatrix} f1 \\ \vdots \\ f13 \end{Bmatrix} \qquad \text{(Eq. 3.6)}$$

where $\hat{A}^T$ represents columns 1 through 12 of A defined by Equation 3.1a and f_i are defined for the equilibrium configuration of the joint element.

The element tangent matrix is defined as the derivative of the residual vector with respect to the external nodal displacements. This matrix is computed from the instantaneous tangents of the joint model components and requires static condensation of the global element tangent matrix:

$$K \cdot \partial U = K \cdot \begin{Bmatrix} \partial u \\ \partial v \end{Bmatrix} = \begin{bmatrix} K_{ee} & K_{ei} \\ K_{ie} & K_{ii} \end{bmatrix} \begin{Bmatrix} \partial u \\ \partial v \end{Bmatrix} = \begin{Bmatrix} \partial F \\ \partial \Phi \end{Bmatrix} = \begin{Bmatrix} \partial R \\ 0 \end{Bmatrix} \quad \text{(Eq. 3.7a)}$$

where

$$K = A^T \cdot k \cdot A \quad \text{(Eq. 3.7b)}$$

and k is the matrix of component tangents as defined in Equation 3.5. Thus, the element consistent instantaneous tangent is defined as follows:

$$\frac{\partial R}{\partial u} = K_{ee} - K_{ei} \cdot [K_{ii}]^{-1} \cdot K_{ie} \quad \text{(Eq. 3.8)}$$

3.4 IMPLEMENTATION OF THE PROPOSED JOINT ELEMENT IN OPENSEES

3.4.1 The OpenSees Framework

OpenSees (**http://opensees.berkeley.edu/**) is an object-oriented open-source software framework for simulation in earthquake engineering using finite element methods. To date, a large number of researchers have enriched this framework with the software components that enable researchers and practicing engineers to accomplish sophisticated simulations of the earthquake response of structures. These components include model-building tools, model domain definitions, element formulations, material models, analysis procedures, numerical solvers, data management tools, and methods to support reliability analysis. Table 3.1 shows some of the classes that compose the software framework, with the classes that are introduced as part of this effort shaded in grey.

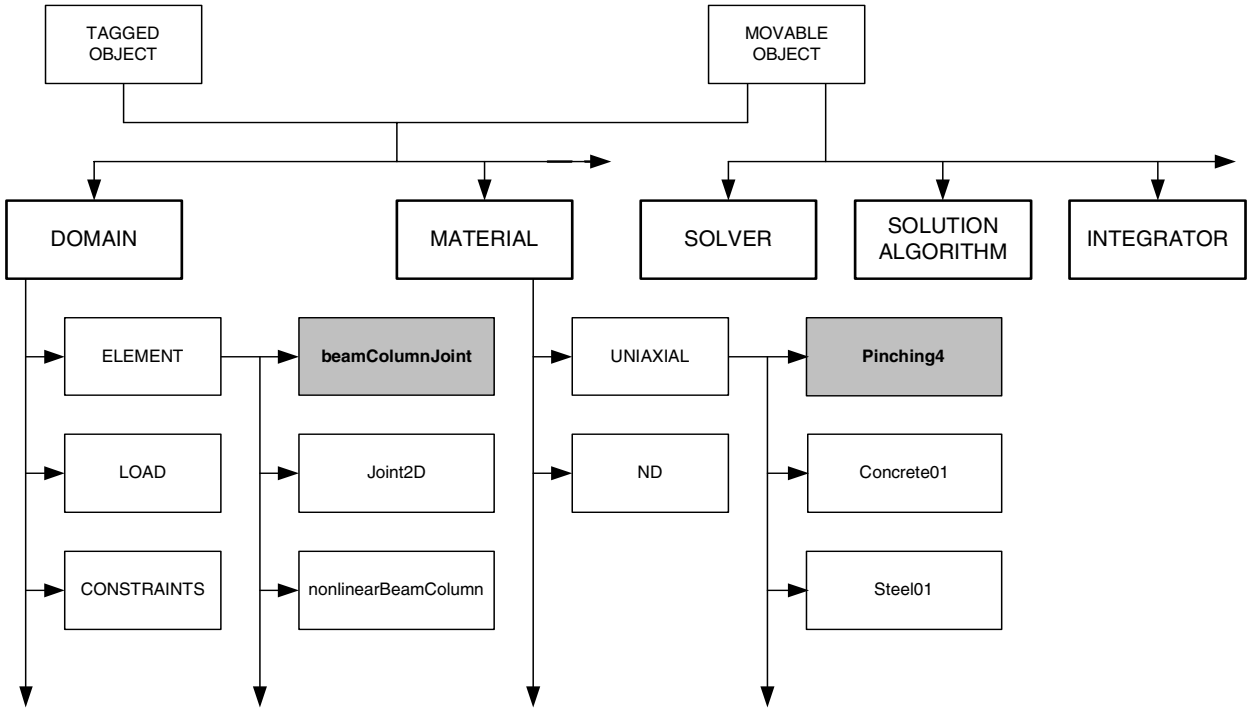

Fig. 3.9. Class structure in the OpenSees framework

3.4.2 The Beam-Column Joint Element

The proposed beam-column joint element formulation is introduced into the OpenSees framework as the ***beamColumnJoint*** class, which is a child of the base abstract ***Element*** class (Fig. 3.9). The ***Element*** class consists of a number of virtual methods that are defined for the children of the class. These methods dynamically allocate and deallocate memory for an instance of the class, initialize an instance of the class, perform inquiry and access tasks, and generate and return an element tangent matrix and residual vector. The proposed beam-column joint element requires an internal solution to determine the internal nodal displacements that satisfy internal equilibrium of the element. Thus, the ***beamColumnJoint*** class includes also multiple methods to support the internal element solution algorithm. Table 3.1 lists and briefly describes all of the methods that compose the ***beamColumnJoint*** class.

Table 3.1. Methods constituting the ***beamcolumnJoint*** Class

Class: beamColumnJoint	
Constructor	
Public: BeamColumnJoint(…)	Initializes an object of the class
Destructor	
Public: ~BeamColumnJoint()	Performs dynamic storage deallocation
Inquiry and Access Methods	
Public: virtual int getNumberExternalNodes()	Returns the number of external nodes of the element
Public: virtual const ID &getExternalNodes()	Returns pointers to the specified node tags
Public: virtual int getNumDOF()	Returns number of degrees of freedom of the element
Public: virtual void setDomain(…)	Required for checking on the dof and associativity with the node
Public: virtual const Matrix &getTangentStiff()	Returns the local stiffness matrix of the element at the global assembly stage for all the elements
Public: virtual const Vector &getResistingForce()	Returns the local residual force vector at the stage of global assembly
Public: virtual int getResponse(…)	Returns element specific responses
Public: virtual int displaySelf(…)	Display element graphically
Element Solution Methods	
Private: void getGlobalDispls(…)	Returns a set of converged displacements (after performing the internal equilibrium check for the beam-column joint) for the four external nodes of the element. This is the main heart of the program which calls in various other methods for its completion
Private: void getBCJoint()	Returns the A matrix being defined in Equation 3.1a. This is a constant matrix for a particular joint and only depends upon the joint dimensions
Private: void getdg_df() & Private: void getdDef_du()	Returns part of the A matrix to be required for performance of the static condensation
Private: void getMatResponse(…)	Takes in the displacements and returns the tangent and residual forces based upon whichever material the user specifies
Private: void formR(…)	Forms the local residual force (R) vector of the element
Private: void formK(…)	Forms the local stiffness matrix (K) of the element
Private: double getStepSize(…)	Determines the step size to be used for line search if there is a convergence problem with the internal equilibrium. This method increases the robustness of the element
Public: virtual int commitState()	Commits the displacement at each nodes once the internal equilibrium criteria for the element is met
Public: virtual int revertToLastCommit()	Return back to its last commited state in case the analysis fails
Public: virtual int revertToStart()	Initialization process for the element at start
Public: virtual int update()	Updates the displacements at the external nodes of the element

4 Constitutive Models

The previously proposed two-dimensional beam-column joint element represents inelastic response through the action of a shear-panel component, bar-slip components, and interface-shear components. Calibration of the model to represent the response of a particular beam-column joint with specific material and design parameters requires definition of the one-dimensional force-deformation response of each of these components. For objective and accurate simulation of beam-column joint response, these calibration procedures must employ fundamental material models and introduce a minimum number of simplifying assumptions about behavior. Here, calibration procedures are proposed for each of the joint-element components that meet these requirements. These procedures employ the results of previous research as is appropriate. To facilitate the calibration process, a general one-dimensional hysteretic load-deformation model is developed. Component calibration procedures define response on the basis of this hysteretic model.

4.1 A GENERAL ONE-DIMENSIONAL CONSTITUTIVE MODEL

Simulation of material and component response in structural analysis applications often includes definition of a one-dimensional hysteretic load-deformation relationship. To facilitate the development and calibration process for the beam-column joint element, a general deformation-based model is proposed that can be calibrated to represent the response of each of the components that compose the joint element. A response envelope, an unload-reload path, and three damage rules that control evolution of these paths define the one-dimensional model. In general, the envelope and unload-reload paths may take any form, in the current implementation, the envelope is multilinear and the unload-reload path is trilinear. Figure 4.1 shows an idealization of a load-deformation history predicted using this model.

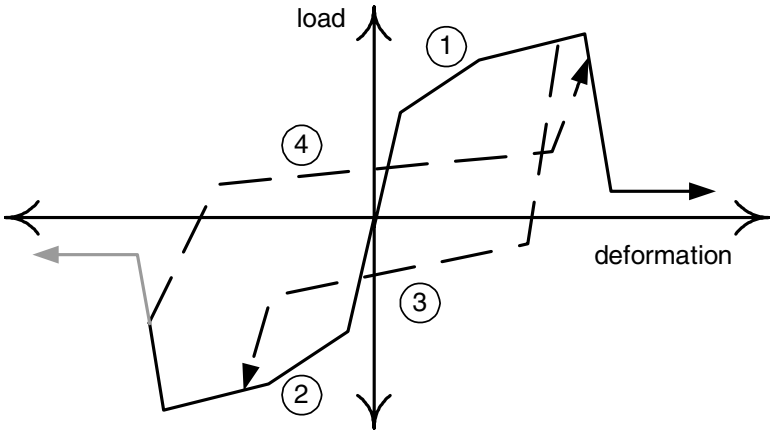

Fig. 4.1 One-dimensional load-deformation response model

The response envelope, unload-reload paths and damage rules define the hysteretic model. For the implementation, shown in Figure 4.1 calibration of the model requires 16 parameters to define the response envelope (material States 1 and 2 in Fig. 4.1), 6 parameters to define the two unload-reload paths (material States 3 and 4 in Fig. 4.1), and 12 parameters to define the hysteric damage rules. The hysteretic model is implemented by defining the four material states, the rules the control changes between states, and the rules that govern evolution of the states.

4.1.1 State Definition

Figure 4.1 shows the four material states that define the proposed hysteretic model. Each state is defined by the same data: the minimum and maximum deformations and associated loads that mark the beginning and end of the state, a loading direction, and a series of rules that define the load path within the state. For State 1 and State 2, the load path changes during an analysis to accommodate strength reduction due to load-deformation history. The load path for State 3 (State 4) is defined each time the state is entered and does not change until the state is exited. For State 3 (State 4), in addition to the maximum (minimum) load-deformation point, defined by the point at which unloading occurs and the minimum (maximum) load-deformation point, defined by the State 3 - State 2 (State 4 - State 1) transition, two load-deformation points define the load path. These load-deformation points include the point reached once substantial unloading has occurred and the point at which substantial reloading occurs. For State 3 (State 4), the load achieved upon unloading is defined as a fraction of the minimum (maximum) strength that can be developed.

With the unloading stiffness defined, this establishes the end of the substantial unload phase. Also for State 3 (State 4), the load-deformation point at which substantial reloading occurs, is a fraction of the minimum (maximum) historic deformation and a fraction of the load developed at the minimum (maximum) deformation demand.

4.1.2 Rules for Change in State

Figure 4.2 shows the connectivity between four material states. The proposed model is a displacement-based model; it is assumed that the model defines the current load and instantaneous tangent to the load-deformation response given the previous material state and an imposed deformation increment. For States 1 and 2, a change in state (CIS) occurs only if there is a reversal in the loading direction; for example, if the current state is State 1 and the current deformation increment is negative, then there is a CIS to State 3 or, if the increment is very large, State 2. For States 3 and 4, a change in the direction of loading or loading beyond the end of the state can trigger a CIS. For example, if the current state is State 3 and the current deformation increment is negative, there may be a CIS to State 2; if the current state is State 3 and the deformation increment is positive, then there is a CIS to State 4 or, if the increment is large, to State 1.

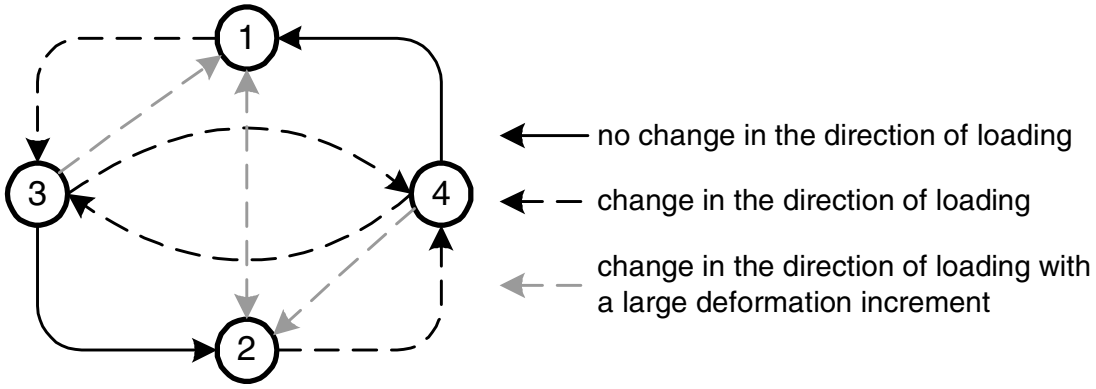

Fig. 4.2. State connectivity

4.1.3 Hysteretic Response

Three damage rules define evolution of the response envelope and unload-reload paths as a function of load-deformation history. Hysteretic damage is simulated through deterioration in

unloading stiffness (unloading stiffness degradation), deterioration in the strength developed in the vicinity of the maximum and minimum deformation demands (reloading stiffness degradation), and deterioration in strength achieved at previously unachieved deformation demands (strength degradation). Figures 4.3, 4.4, and 4.5 show the impact of these three different damage modes on the hysteretic material response.

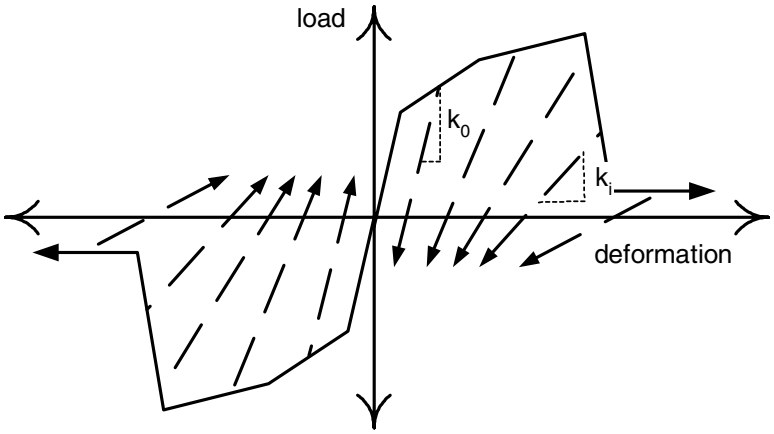

Fig. 4.3. Unloading stiffness degradation

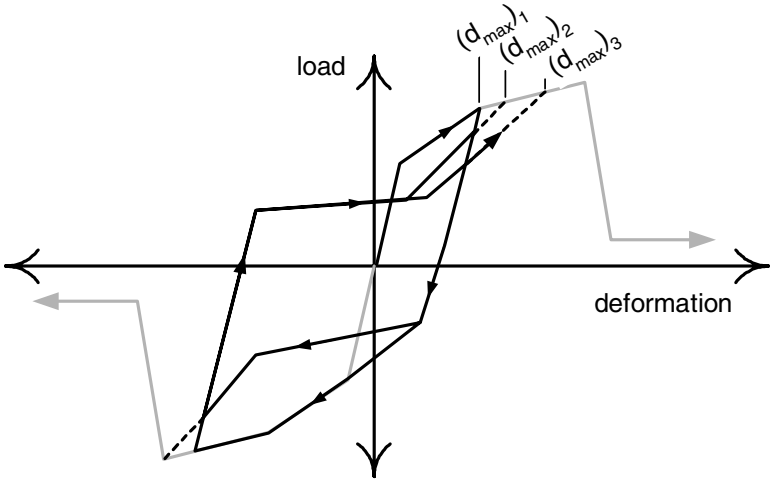

Fig. 4.4. Reloading stiffness degradation

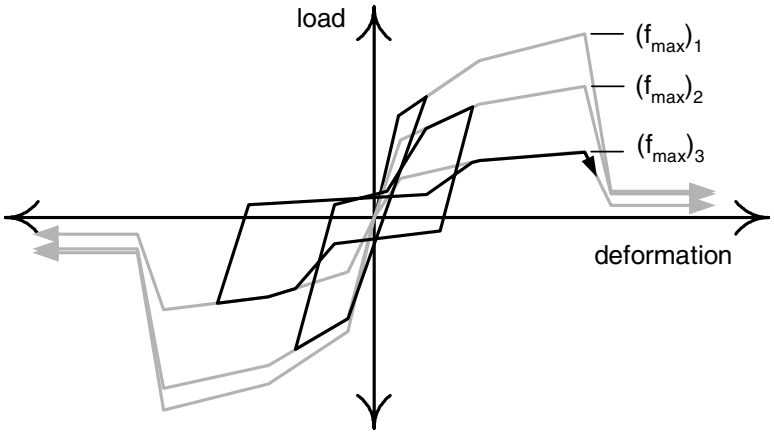

Fig. 4.5. Strength degradation

The form of each damage rules is the same; this form represents a more general version of the damage index proposed by Park and Ang [1985].

$$\delta_i = \left(\alpha 1 \cdot \left(\tilde{d}_{\max} \right)^{\alpha 3} + \alpha 2 \cdot \left(\frac{E_i}{E_{monotonic}} \right)^{\alpha 4} \right) \qquad \text{(Eq. 4.1a)}$$

where

$$\tilde{d}_{\max} = \max \left[\frac{d_{\max i}}{def_{\max}}, \quad \frac{d_{\min i}}{def_{\min}} \right] \qquad \text{(Eq. 4.1b)}$$

$$E_i = \int_{load\ history} dE \qquad \text{(Eq. 4.1c)}$$

and i refers to the current displacement increment, δ_i is the damage index (δ_i equal to 0 represents a state of no damage and δ_i equal to 1.0 represents the case of maximum damage), α's are parameters used to fit the damage rule to the experimental data, E is hysteretic energy with $E_{monotic}$ equal to the energy required to achieve under monotonic loading the deformation that defines failure, def_{max} and def_{min} are, respectively, the positive and negative deformations that define failure, and d_{max_i} and d_{min_i} are, respectively, the maximum historic and minimum historic deformation demands.

For the case of stiffness degradation:

$$k_i = k_0 \cdot (1 - \delta k_i) \qquad \text{(Eq. 4.2)}$$

where k_i is the current unloading stiffness (Fig. 4.3), k_0 is the initial unloading stiffness for the case of no damage (Fig. 4.3), and δk_i is the current value of the stiffness damage index. Envelope strength degradation is simulated in the same way:

$$(f_{\max})_i = (f_{\max})_0 \cdot (1 - \delta f_i) \quad \text{(Eq. 4.3)}$$

where $(f_{\max})_i$ is the current envelope maximum strength (Fig. 4.5), $(f_{\max})_0$ is the initial envelope maximum strength for the case of no damage (Fig. 4.5), and δf_i is the current value of the strength damage index. The reduction in strength that is observed upon reloading is simulated by applying the damage rule to define an increase in the maximum historic deformation (decrease in the minimum):

$$d_{\max i} = d_{\max 0} \cdot (1 + \delta d_i) \quad \text{(Eq. 4.4)}$$

where $d_{\max i}$ is the current deformation that defines the end of the reload cycle for increasing deformation demand (Fig. 4.4), $d_{\max 0}$ is the maximum historic deformation demand (Fig. 4.4), and δd_i is the current value of the reloading-strength damage index.

4.1.4 Implementation of the General Hysteretic Constitutive Model in OpenSees

As shown in Figure 3.9, the base abstract ***Material*** class is one of the primary classes making up the OpenSees framework. Children of the ***Material*** class include the base abstract ***UniaxialMaterial*** class, children of which represent implementations of one-dimensional material constitutive models, and the base abstract ***ND*** class, children of which represent implementations of multi-dimensional material constitutive models. The ***Material*** and ***UniaxialMaterial*** classes comprise a number of virtual methods that are defined in the children. These methods dynamically allocate and deallocate memory for an instance of the class, initialize an instance of the class, perform inquiry and access tasks, and generate and return a material tangent matrix and generalized stress vector.

The proposed general one-dimensional constitutive model is introduced into the OpenSees framework as the ***Pinching4*** class, a child of the abstract ***UniaxialMaterial*** class (Fig. 3.9). In addition to including definitions of virtual methods inherited from the abstract Material and UniaxialMaterial classes, the ***Pinching4*** class includes also a number of private methods that define the current state of the material. Table 4.1 lists and briefly describes all of the methods that make up the ***Pinching4*** class.

Table 4.1. Methods constituting the ***Pinching4*** class

Class: Pinching4	
Constructor	
Public: BeamColumnJoint(…)	Initializes an object of the class
Destructor	
Public: ~BeamColumnJoint()	Performs dynamic storage deallocation
Inquiry & Access Methods	
Public: virtual double getStrain()	Returns the current converged strain/displacement of the material
Public: virtual double getStress()	Returns current converged stress/force of the material
Public: virtual double getTangent()	Returns current converged tangent of the material
Public: virtual UniaxialMaterial* getCopy()	Performs deep copy of the material object
Material Solution Methods	
Public: virtual int setTrialStrain(…)	Sets a displacement demand of the material based upon its previous stiffness and also the residual force vector return
Private: void setEnvelope()	Sets the initial backbone envelope for the material based upon the input by the user
Private: void getState(…)	Determines the state of the material based upon the material history and current stress demand
Private: double posEnvlpStress(…) & Private: double negEnvlpStress(…)	Returns positive/negative damaged stress of the material
Private: double posEnvlpTangent(…) & Private: double negEnvlpTangent(…)	Returns positive/negative tangent of the material
Private: void getState3(…) & Private: void getState4(…)	Forms the backbone envelope of state 3 / state 4 of the material model
Private: double Envlp3Stress (…) & Private: double Envlp4Stress ()	Determines the stress of the envelope at state 3 or state 4 of the material
Private: double Envlp3Tangent (…) & Private: double Envlp4Tangent (…)	Determines the tangent of the envelope at state 3 or state 4 of the material
Private: void updateDmg(…)	Determines the damages at a particular state of the material.
Public: virtual int commitState()	Commits the history variables of the material model after the state-check has been done for the material model
Public: virtual int revertToLastCommit()	Return back to its last commited state in case the analysis fails
Public: virtual int revertToStart()	Initialization process for the material at start

4.2 MODELING BAR-SLIP RESPONSE

Figure 3.3 shows an idealization of the joint core load distribution under earthquake loading of a building frame. This load distribution results in substantial bond demand for frame-member longitudinal reinforcement anchored in the beam-column joint (light gray arrows indicate load transferred from reinforcing steel to joint core through bond Fig. 3.3). A calibration procedure is developed to simulate the inelastic response associated with bond-zone deterioration.

One possible approach for developing a calibration model to use in defining the bar stress versus slip relationship is to use data from experimental testing of beam-column joint

subassemblies with different material properties, geometries, configurations, design properties, and load histories. However, experimental measurement of bar slip requires a relatively sophisticated instrumentation set-up and the adoption of a definition as to what constitutes slip. Calculation of experimental bar stress requires the use of steel strain gage data and an assumed hysteretic material model or an assumption about the stress distribution across the beam or column cross section. These factors limit the availability of experimental data, the objectivity of the available data, and the generality of a model developed on the basis of these data.

A second possible approach to model calibration, used in the current study, employs data from experimental testing of anchorage-zone specimens and assumptions about the bond stress distribution within the joint. This approach enables the use of a much larger data set and provides a bar stress versus slip model that can be applied in general for simulating beam-column joint response.

4.2.1 Envelope of the Bar Stress versus Slip Relationship

In the current study, the envelope to the bar stress versus slip relationship is developed on the basis of several simplifying assumptions about beam-column joint anchorage-zone response. First, bond stress along the anchored length of a reinforcing bar is assumed to be uniform for reinforcement that remains elastic or piecewise constant for reinforcement loaded beyond yield (Fig. 4.6). Second, slip is assumed to define the relative movement of the reinforcing bar with respect to the face of the beam-column joint and is a function of the steel strain distribution along the bar. Third, the bar exhibits zero slip at the point of zero bar stress. This approach is similar to that used by Mazzoni and Moehle [2001]. Figure 4.6 shows an idealization of the bond stress distribution and resulting bar stress distribution for an anchored reinforcing bar loaded in tension beyond yield. Parameters identified in the figure are defined in the following paragraph.

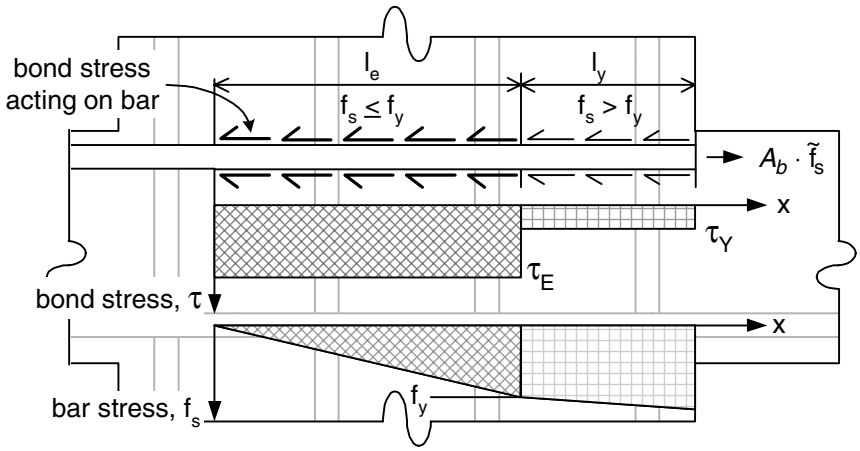

Fig. 4.6. Bond and bar stress distribution for a reinforcing bar anchored in a joint

On the basis of these assumptions, the slip versus bar stress relationship is defined by the following equations:

$$\text{for } \tilde{f}_s < f_y$$

$$slip = \int_0^{l_{fs}} \tau_E \frac{\pi d_b}{A_b} \cdot \frac{1}{E} x dx = 2 \frac{\tau_E}{E} \frac{{l_{fs}}^2}{d_b} = \frac{1}{8} \frac{\tilde{f}_s^{\,2}}{\tau_E \cdot E} d_b \qquad \text{(Eq. 4.5a)}$$

$$\text{for } \tilde{f}_s \ge f_y$$

$$\begin{aligned} slip &= \int_0^{l_e} \frac{4}{d_b} \frac{\tau_E}{E} x dx + \int_{l_e}^{l_y + l_e} \frac{f_y}{E} + \tau_Y \frac{4}{d_b} \frac{1}{E_h} (x - l_e) dx \\ &= 2 \frac{\tau_E}{E} \frac{(l_e)^2}{d_b} + \frac{f_y}{E} l_y + 2 \frac{\tau_Y}{E_h} \frac{(l_y)^2}{d_b} \\ &= \frac{1}{8} \frac{f_y}{\tau_E} \frac{f_y}{E} d_b + \frac{1}{4} \frac{\tilde{f}_s - f_y}{\tau_Y} \frac{f_y}{E} d_b + \frac{1}{8} \frac{\left(\tilde{f}_s - f_y\right)^2}{\tau_Y \cdot E_h} d_b \end{aligned} \qquad \text{(Eq. 4.5b)}$$

with

$$l_{fs} = \frac{\tilde{f}_s}{\tau_{ET}} \cdot \frac{A_b}{\pi d_b}, \; l_e = \frac{f_y}{\tau_{ET}} \cdot \frac{A_b}{\pi d_b} \text{ and } l_y = \frac{\tilde{f}_s - f_y}{\tau_{YT}} \cdot \frac{A_b}{\pi d_b} \qquad \text{(Eq. 4.5c)}$$

where f_y is the steel yield strength, E is the steel elastic modulus, E_h is the steel hardening modulus assuming a bilinear stress-strain response, τ_E is the bond strength for elastic steel, τ_Y is the bond strength for yielded steel, A_b is the nominal bar area and d_b is the nominal bar diameter. For the case of $l_e + l_y$ greater than the anchorage length of the joint, deterioration of bond strength under reversed cyclic loading will be much more severe. In this case, it may be appropriate to assume reduced bond strength in the elastic region of the reinforcing bar. Additionally, bond

strength is assumed to deteriorate once slip exceeds a "slip limit" defined on the basis of experimental data.

Bond-strength values, required to complete calibration of the model, are defined on the basis of experimental data provided by a number of different researchers. The results of previous research indicate that bond strength is a function of the material state of the anchored bar as well as of the concrete and transverse reinforcing steel in the vicinity of the reinforcing bar [Lowes 1999]. Bond strength is relatively high if reinforcement is anchored in a reinforced concrete zone that carries compression perpendicular to the bar axis, and relatively low if the reinforced concrete carries tension [Eligehausen et al. 1983; Malvar 1992]. Further, bond strength is reduced for reinforcement carrying stress in excess of the tensile yield strength and increased for reinforcement carrying compressive stress less than the compressive yield strength [Shima et al. 1987].

These factors are considered in defining bond strength for the current model. Figure 3.3 shows a simplified idealization of the load distribution within a building beam-column joint. In the vicinity of the column and beam tension zone, relatively low bond strengths could be expected due to the stress state of the reinforced concrete joint as well as likely tensile yielding of beam reinforcement. Similarly, in the vicinity of the column and beam compression zones, relatively high bond strengths could be expected due to the stress state of the joint and the likely compressive yielding of beam reinforcement.

The results of the experimental investigation by Eligehausen et al. [1983] are used as a basis for defining the bond strength for an elastic reinforcing bar loaded in tension (Table 4.2). For a beam longitudinal reinforcing bar anchored in a building beam-column joint and stressed in tension to a level that does not exceed the yield stress, the concrete in the vicinity of the bar could be expected to carry compression or tension with limited crack width (Fig. 3.3). These bond-zone conditions would not be expected to reduce significantly bond strength from values obtained in typical bond studies, such as the Eligehausen study, that use specimens with short anchorage lengths and initially undamaged bond-zone concrete. The prototype specimen in the Eligehausen study consisted of a No. 8 reinforcing bar (nom. diameter = 1 in. [25 mm]) anchored with a short embedment length in a reinforced concrete anchorage block with a moderate volume of transverse reinforcement and no active confining pressure. Eligehausen et al. proposed a peak bond-strength value of $\tau_{max} = 2.5\sqrt{f_c}$ MPa ($30\sqrt{f_c}$ psi) and a bond stress versus slip model that

implies the average bond-strength values listed in Table 4.2, assuming that zero and the maximum bond strength are developed along the length of anchored bar.

Table 4.2. Average bond strengths as a function of steel stress state

Bar stress, fs (fy = tensile yield strength)	Average bond strength MPa (f_c in MPa)	Average bond strength, psi (f_c in psi)
Tension, fs < fy	$\tau_{ET} = 1.8\sqrt{f_c}$	$\tau_{ET} = 21\sqrt{f_c}$
Tension, fs > fy	$\tau_{YT} = 0.4\sqrt{f_c}$ to $0.05\sqrt{f_c}$	$\tau_{YT} = 4.8\sqrt{f_c}$ to $0.6\sqrt{f_c}$
Compression, -fs < fy	$\tau_{EC} = 2.2\sqrt{f_c}$	$\tau_{EC} = 26\sqrt{f_c}$
Compression, -fs > fy	$\tau_{YC} = 3.6\sqrt{f_c}$	$\tau_{YC} = 43\sqrt{f_c}$

Average bond strength for the region of the reinforcing bar that yields in tension is defined on the basis of experimental data provided by Shima et al. [1987] and Eligehausen et al. [1983]. The prototype specimen in the Shima investigation consisted of a No. 19M (nom. diameter = 19.5 mm [0.88 in.]) reinforcing bar embedded in a plain concrete cylinder with an embedment length of 50 bar diameters. Bond strength along the length of the bar was computed from strain gage data and an experimentally determined steel stress-strain relationship. The results of this study indicate average bond strength for yielded reinforcement of $0.4\sqrt{f_c}$ MPa ($4.8\sqrt{f_c}$ psi) (Table 4.2). The Shima test specimens consist of initial undamaged concrete cylinders and thus do not represent the relatively poor bond zone conditions that exist for yielded reinforcing bars anchored in the vicinity of beam and column flexural tension zones. This could be expected to reduce bond strength further. Eligehausen et al. [1983] propose a model in which maximum bond strength for reinforcement anchored in the vicinity of a flexural tension zone is 40% of that proposed for reinforcement anchored within an undamaged and well-confined anchorage zone. However, Eligehausen et al. [1983] observed minimum bond strength of $0.05\sqrt{f_c}$ MPa ($0.6\sqrt{f_c}$ psi) for nonyielded reinforcement embedded in a damaged anchorage zone. These damaged anchorage zones are more representative of anchorage zones conditions in the vicinity of flexural tension zones. These two maximum bond-strength values are assumed to bound the range of values.

The anchorage of reinforcement embedded in concrete elements subjected to active and passive confining pressure has been studied by a number of researchers [Eligehausen et al. 1983; Malvar 1992]. However, the majority of these investigations have been for reinforcement loaded in tension. The results of the Eligehausen investigation show that bond strength does not vary for

reinforcing bars carrying compressive or tensile stress below the yield strength. Thus, studies for reinforcement loaded in tension are used as a basis defining the average bond strength for joint reinforcement carrying compression and thus anchored in a beam or column compression zone. Evaluation of bond data indicates that peak local bond strength of $3.1\sqrt{f_c}$ MPa with f_c in MPa ($37\sqrt{f_c}$ psi with f_c in psi) may be developed for confining pressure equal to 40% of concrete compressive strength [Lowes 1999]. Assuming that this maximum bond strength is developed and assuming the same bond stress versus slip model as for reinforcement loaded in tension, the average bond-strengths values listed in Table 4.2 are computed.

For the case of a reinforcing bar yielded in compression, and thus anchored in the vicinity of a flexural compression zone, the results of an investigation by Viwathanatepa et al. [1979] and the Eligehausen investigation [Eligehausen et al. 1983] are considered. For the Viwathanatepa study, a typical laboratory test specimen consisted of a No. 8 reinforcing bar (nom. diameter = 25 mm = 1 in.) embedded in an idealized reinforced concrete column with an anchorage length of $25d_b$ and subjected to tension and compression loading on either end of the embedded bar. The test configuration was such that the tension end of the reinforcing bar was anchored in the vicinity of the column flexural tension zone while the compression end of the bar was anchored in the compression zone. While peak bond strength in excess of $6\sqrt{f_c}$ MPa with f_c in MPa ($72\sqrt{f_c}$ psi with f_c in psi) is reported for yielded reinforcement anchored in the flexural compression zone, the observed response is simulated using a model with a peak bond strength of $3.8\sqrt{f_c}$ MPa with f_c in MPa ($46\sqrt{f_c}$ psi with f_c in psi). This peak bond strength is proposed for use in simulation also by Eligehausen et al. The Eligehausen investigation arrives at this strength by increasing by 20%, to account for Poisson's effect, the maximum observed bond strength for bars anchored in compression zones. Here it is assumed that local slip levels for reinforcement yielding in compression approach those associated with maximum bond strength; thus, the value for peak bond strength proposed by the Viwathanatepa and Eligehausen studies defines average bond strength in the current study (Table 4.2).

The average bond-strength values listed in Table 3.1 are used to calibrate the piecewise linear envelope to the bar stress versus slip relationship. Definition of the envelope is completed by identification of the slip level at which bond strength begins to deteriorate and the post-peak stiffness of the envelope. Here the slip limit is defined to be 3 mm (0.1 in.); this follows the recommendations of Eligehausen et al. [1983] and is consistent with the results of previous

studies [Lowes 1999]. The post-peak stiffness is defined to be -10% of the initial elastic stiffness; this is assumed to represent the local post-peak stiffness observed by Eligehausen et al.

The proposed model may be compared with experimental data defining bar stress versus slip response for anchorage-zone specimens with relatively long anchorage lengths and variable anchorage-zone conditions. Experimental tests conducted by Viwathanatepa et al. [1979] provide the most comprehensive data set for this type of bond specimen. Figure 4.7 shows the proposed bar stress versus slip envelope as well as envelopes computed from experimental data provided by Viwathanatepa et al. for the case of monotonic loading and reversed cyclic loading. The simulated response history lies between that observed for monotonic and cyclic loading. The previously discussed damage rules are calibrated to improve simulation of observed response under reversed-cyclic loading. However, the data in Figure 4.7 suggest that the model may not be appropriate for use in simulating response under purely monotonic loading.

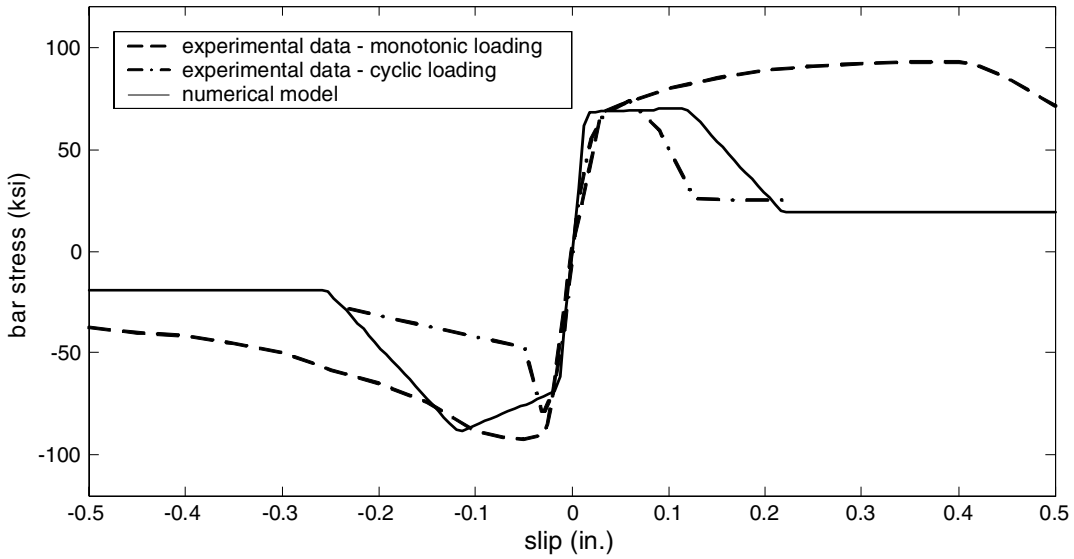

Fig. 4.7. Envelope for hysteretic bar-slip versus slip response, experimental data from Viwathanatepa et al. [1979]

4.2.2 Cyclic Response

Extension of the monotonic bar stress versus slip history for the case of reversed-cyclic loading requires definition of the unload-reload path and definition of a damage model to represent the influence of load history on response. The results of reversed-cyclic anchorage tests conducted by Eligehausen et al. [1983] and Hawkins et al. [1982] are used as the basis for defining these response characteristics. These data show bar stress versus slip response histories that are similar

in nature to those observed by Viwathanatepa et al. [1979] and shown in Figure 4.8a. Experimental data show that the hysteretic bar stress versus slip response is characterized by a stiff unloading response, the development of a residual bond-slip resisting force upon slip reversal, and a pinching-type response in which bar stress does not increase significantly until slip demand approaches the maximum slip demand achieved during previous load cycles. Additionally, experimental data indicate that bond strength and stiffness deteriorates as a function of the load history. Figure 4.1 shows the one-dimensional hysteretic model used to simulate observed response. Calibration of this model requires specification of the following parameters:

- Unloading stiffness: assumed equal to the elastic stiffness
- Residual bar stress: computed assuming that a uniform residual bond stress of $0.15\sqrt{f_c}$ MPa with f_c in MPa ($1.8\sqrt{f_c}$ psi with f_c in psi) to represent data provided by Eligehausen et al. [1983]
- Slip and force at which reloading occurs as a fraction of maximum historic slip and force associated with maximum historic slip: defined to be 0.25 to represent Eligehausen and Hawkins data

4.2.3 Comparison of Simulated and Observed Response

Calibration of the model also requires specification of a set of eight cyclic-degradation parameters that define deterioration of strength and stiffness under cyclic loading. These parameters are defined to represent the Eligehausen et al. [1983] and Hawkins et al. [1982] data. Figure 4.8 shows the proposed model compared with experimental bar stress versus slip data presented by Viwathanatepa et al. [1979]. The proposed model represents the general characteristics of the observed response. Discrepancies between simulated and observed response result from the simplicity of the model.

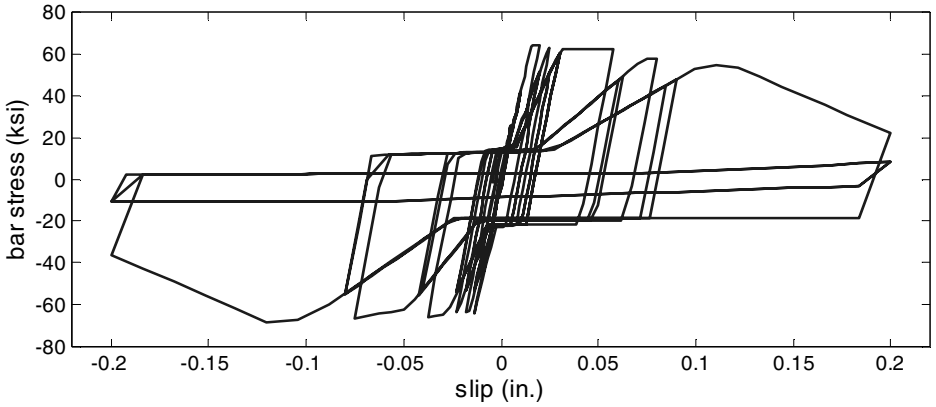

(a) Simulated response

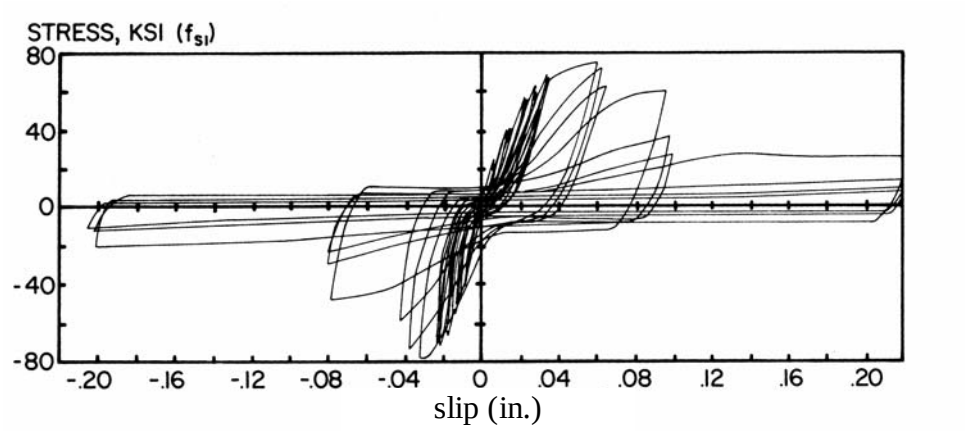

(b) Observed response (Fig. 4.14 from Viwathanatepa et al. [1979])

Fig. 4.8. Simulated and observed bar stress versus slip for anchored reinforcing bar

4.2.4 Spring-Force versus Bar Stress Calibration Model

Calibration of the bar-slip springs included in the beam-column joint model is completed by definition of a bar stress versus spring-force relationship. The tensile and compressive spring forces equilibrate the axial and flexural loads carried by the beams and columns framing into the joint. The bar stress defines the load carried by the framing member longitudinal reinforcement. This load is transferred into the joint through bond and, thus, determines the additional joint flexibility associated with bond-zone damage. For the case of a tensile spring force, it is appropriate to assume that all of the spring force is carried by the reinforcing steel and transferred through bond. However, for the case of a compressive spring force, the load is distributed between the concrete and reinforcing steel. Thus, only a fraction of the total spring force is transferred into the joint through bond. To define the spring force versus bar stress

relationship for this case, the fraction of the cross-section compression resultant force carried by the reinforcing steel for loading at nominal flexural strength is assumed to be valid for all load distributions.

In determining the relationship between compressive resultant spring force and bar stress, the assumed behavioral mechanisms of the beam-column joint belie all but the simplest models. Thus, spring force and bar stress are related on the basis of an assumed stress-strain distribution on the frame-member cross section for the case of the loading to nominal flexural strength. This stress-strain distribution follows the recommendations of ACI Committee 318 [1999] for calculation of nominal flexural strength and is depicted in Figure 4.9. Using this model, concrete and steel force resultants are defined as follows:

$$C_c = 0.85 f_c^{'} \beta c w \qquad \text{(Eq. 4.6a)}$$

$$C_s^{'} = f_s^{'} A_s^{'} = 0.003 \frac{c - d^{'}}{c} E_s A_s^{'} \qquad \text{(Eq. 4.6b)}$$

where C_c is total compressive force carried by the concrete and $C_s^{'}$ is the total compressive force carried by the reinforcing steel, $A_s^{'}$ is the area of reinforcing steel-carrying compression, E_s is the reinforcing steel elastic modulus and all other parameters are defined in Figure 4.9. Assuming that the centroid of the compression force is defined by the concrete stress distribution, the compressive spring force is defined, as a function of the compressive bar stress, as follows:

$$spring\ force = C_s^{'} + C_c = f_s^{'} A_s^{'} \left(1 + \frac{0.85 f_c^{'} d w}{E_s A_s^{'}} \frac{2(1-j)}{0.003 \beta \left(1 - \frac{d^{'}}{d} \frac{\beta}{2(1-j)} \right)} \right) \qquad \text{(Eq. 4.7)}$$

The parameters used in Equation 3.7 are defined in Figure 4.9. From Equation 3.7 it follows that assuming a constant ratio of spring force to bar force implies assuming that *jd,* and thus the neutral axis depth, is constant. This assumption is made often for design, and the following values are appropriate:

$j = 0.85$ for beams

$j = 0.75$ for columns

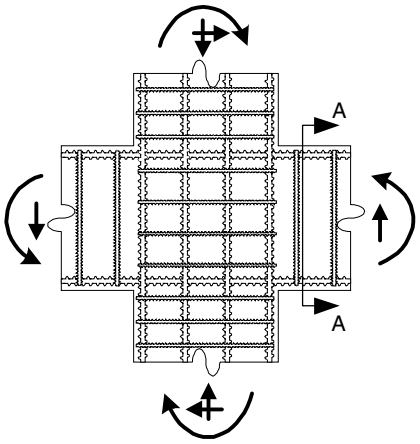

(a) RC frame member loads in the vicinity of a beam-column joint

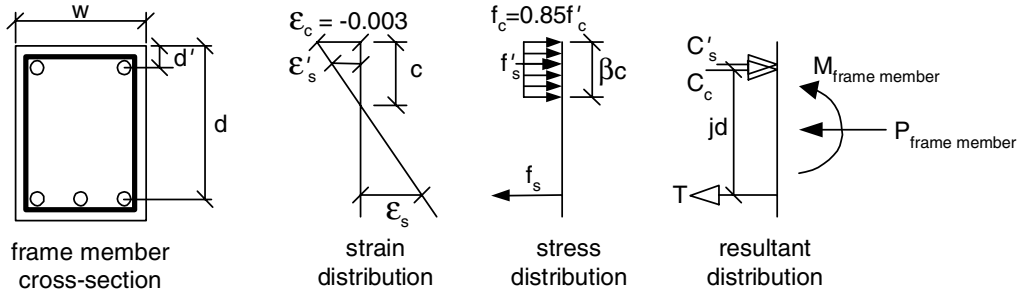

(b) Section A-A: Strain, stress and resultant distribution

Fig. 4.9. Idealization of frame-member internal load distribution at joint perimeter

For the case of tensile resultant force acting on the frame-member cross-section, concrete does not contribute to the transfer of load into the joint. Thus, all tensile loads are carried by the reinforcing steel and transferred into the joint through bond. For tensile loading of the bar-slip spring the relationship between spring force and bar stress is as follows (Fig. 4.9):

$$T = f_s A_s \qquad \text{(Eq. 4.8)}$$

where T is the tensile resultant acting on the cross section equal to the spring force, f_s is the reinforcing bar stress, and A_s is the total area of reinforcing steel.

4.3 MODELING JOINT SHEAR RESPONSE

Figure 3.3 shows an idealization of the loads applied to the joint core under earthquake loading of a frame. This load distribution results in substantial shear loading of the joint-core concrete. Depending on bond-zone conditions, the load distribution at the perimeter of the joint core may

be relatively uniform, or shear may be transferred primarily through concrete compression and bond forces in the vicinity of the beam and column flexural compression zones. A calibration procedure is developed to simulate the inelastic load-deformation response of the joint core under the applied shear load.

Evaluation of experimental data characterizing the response of beam-column joint subassemblages is one possible approach for development of a general calibration procedure for the shear panel component. However, there are relatively few data sets for joints with different material properties, geometries, design parameters, and cyclic load histories. Additionally, different researchers use different approaches to measure shear deformation of the joint region. Instrumentation layouts that include bond zones within the joint, flexural yield zones in beams and columns, or highly localized regions of the joint likely overpredict shear deformation of the joint core concrete. Further, bond-zone conditions determine the distribution of the shear loading of the joint core and may determine the shear stress history. Thus, development of a calibration model requires comparison of data sets with similar bond-zone conditions. These factors limit the data that are appropriate for model development, and thus the generality of a model developed solely on the basis of these data.

In the current study, experimental data characterizing the response of plain and reinforced concrete components subjected to uniform shear loading are used as a basis for modeling the shear-panel response. A simple calibration model is developed that employs the modified compression field theory (MCFT) [Vecchio and Collins 1986] to define the envelope to the shear stress versus strain history of the joint core and experimental data provided by Stevens et al. [1991] to define the response under cyclic loading.

4.3.1 Calibration of the Shear-Panel Component

Vecchio and Collins [1986] tested reinforced concrete panels with different material properties and transverse steel ratios under monotonic shear and combined shear and axial loading. Using these data, Vecchio and Collins developed the MCFT to characterize the global response of the panels. This theory defines a plane-stress constitutive model for reinforced concrete elements in which failure is determined by yielding of reinforcement at concrete crack surfaces or by crushing of previously cracked concrete.

For beam-column joints in a two-dimensional frame, the joint experiences essentially planar shear loading. The failure mechanisms observed in the laboratory for joints subjected to

simulated earthquake loading are those represented by the MCFT. Also, application of the MCFT enables calibration of the joint panel response model as a function of concrete material properties, vertical and horizontal steel ratios in the joint, and steel reinforcement material properties. For these reasons, the MCFT is proposed for use in calibrating the shear-panel component of the beam-column joint element.

Several issues must be addressed in order to apply the MCFT to generate an envelope to the shear stress versus strain response history. First, application of the theory requires the introduction of some assumptions regarding the axial and flexural response of the beam-column joint. Here it is assumed that all load transferred through the joint occurs through shear. Also, it is assumed that axial and flexural deformations are negligible. Second, as proposed by Vecchio and Collins [1986], the MCFT characterizes the response of a panel subjected to monotonic loading; thus, the MCFT must be extended to represent the response under cyclic loading. A subsequent study [Stevens et al. 1991] extends the MCFT for the case of reversed-cyclic loading; however, this constitutive model provides an inappropriately high level of accuracy, resolution, and sophistication given the simplicity of the proposed beam-column joint element. Instead, for the current study, only the response envelope is defined using the MCFT, and experimental data provided by Stevens et al. are used to calibrate the unload-reload paths of the general hysteretic response model. The results of the Steven's study include the observation that for panels subjected to reversed cyclic shear loading, concrete compressive strength is substantially less than that observed under monotonic loading and that concrete tensile strength deteriorates more rapidly as a function of tensile strain. Using the concrete compressive strength reduction factor proposed by Stevens et al. and a concrete tensile stress-strain response model derived from the Stevens data these characteristics are incorporated into the current model.

Figure 4.10 shows the simulated response history for two panels subjected to monotonic loading as predicted using the MCFT. These panels, designated Panel 1 and Panel 2, have material and geometric properties listed in Table 4.3 The response of Panel 1 is determined by yielding of the transverse reinforcement while the response of Panel 2 is determined by crushing of the concrete. These response histories are assumed to constitute the envelope to the panel shear stress versus strain response for the case of monotonic loading of beam-column joints.

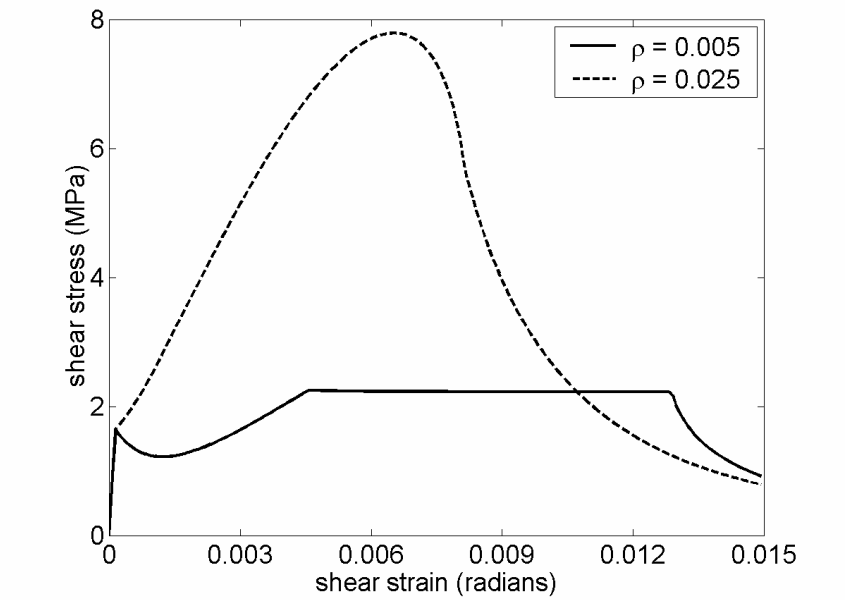

Fig. 4.10. Simulated shear stress versus strain response history for monotonic loading

Table 4.3 Material and geometric properties used in simulations

Specimen	Concrete Material Properties			Steel Material Properties					
	Compressive Strength (MPa)	Strain at Compressive Strength (MPa)	Tensile Strength (MPa)	ρ_x	ρ_x	Elastic Modulus (MPa)	Yield Strength (MPa)	Hardening Modulus (MPa)	Ultimate Strength (MPa)
Panel 1	-25	-0.002	1.65	0.005	0.005	2.07e+05	414	2.07e+03	455
Panel 2	-25	-0.002	1.65	0.025	0.025	2.07e+05	414	2.07e+03	455
SE8	-37	-0.0026	2.01	0.0293	0.0098	2.07e+05	492 (ρ_x) 479 (ρ_y)	2.07e+03	541 (ρ_x) 526 (ρ_y)
SE9	-44.2	-0.00265	2.19	0.0293	0.0098	2.07e+05	422	2.07e+03	464
BCJ4	-27.6	-0003	1.73	0.0137	0.017	2.07e+05	414	2.07e+03	455

4.3.2 Cyclic Response

Calibration of the shear-panel component is completed by characterization of the entire reversed-cyclic response history. Like other data characterizing cyclic shear response of RC elements [Leon 1990], the Stevens data [Stevens et al. 1991] show an extremely pinched stress-strain history. This behavior is attributed to opening and closing of cracks in the concrete-steel composite. This behavior is represented using the proposed general hysteretic response model with unloading response defined to be equal to the initial elastic stiffness and reloading defined to occur at a shear strain equal to approximately 25% of the maximum historic shear strain demand and shear strength of zero.

4.3.3 Comparison of Simulated and Observed Response

Relatively few experimental investigations consider the response of reinforced concrete elements subjected to uniform shear loading; thus, data for use in model validation are limited. Figure 4.11a shows the linear interpolation of the monotonic envelope, as defined using the MCFT model, and the simulated response for the case of reversed cyclic loading. These data may be compared with the experimental data used to calibrate the model (Fig. 4.11b). Figure 4.12 shows simulated and observed response for a second panel tested by Stevens et al. [1991]. Discrepancies result from the relative simplicity of the proposed model, definition of experimental joint shear stress, and an instrumentation setup for measuring of joint shear strain that includes deformation of the reinforcement anchorage zones.

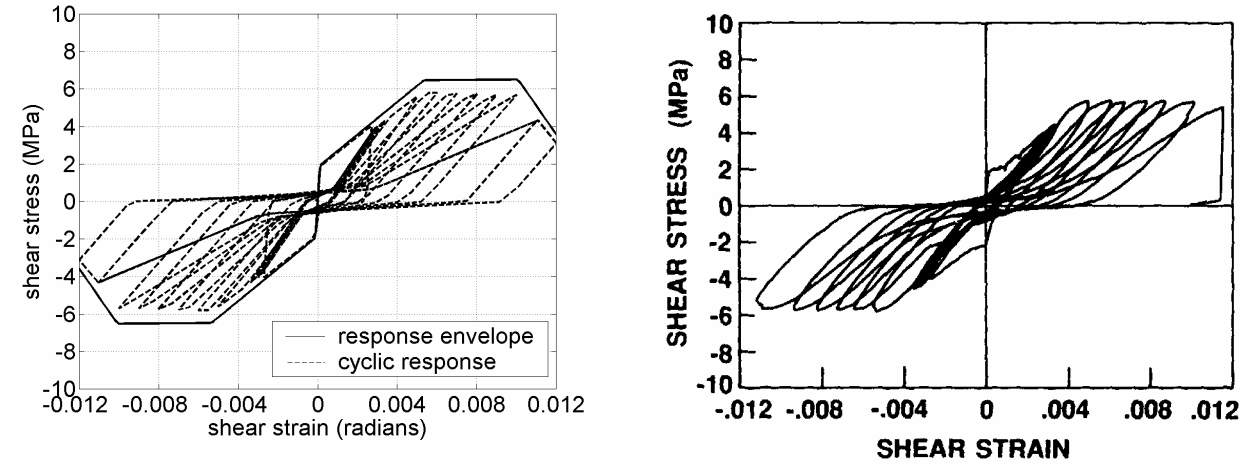

(a) Simulated response (b) Observed response

Fig. 4.11. Behavior of reinforced concrete Panel SE8 tested by Stevens et al. [1990]

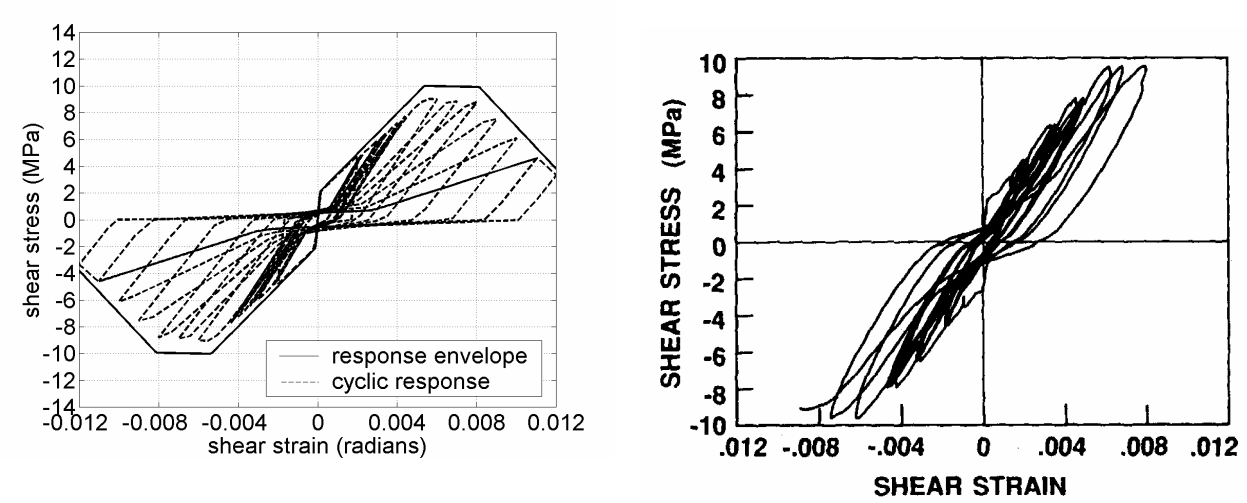

(a) Simulated response (b) Observed response

Fig. 4.12. Behavior of reinforced concrete Panel SE9 tested by Stevens et al. [1990]

4.4 MODELING INTERFACE-SHEAR RESPONSE

Under earthquake loading of a building frame (Fig. 3.3), flexural cracks will open in beams, and possibly columns, near the perimeter of the beam-column joint. If earthquake loading or bond-strength deterioration is severe, cracks may not close upon load reversal and may widen with subsequent load cycles. Experimental investigation [Ma et al. 1976] indicates that as these cracks widen, the capacity for shear transfer across the crack surface decreases and the flexibility of this shear transfer mechanism increases. This behavior is represented by the interface shear components of the beam-column joint element (Fig. 3.4).

Shear transfer in reinforced concrete occurs through compression-strut action, dowel action of reinforcing steel and aggregate interlock on cracked concrete surfaces. For the beam-column joint model, it is assumed that if concrete cracks at the perimeter of the joint are closed (defined by compressive deformation of one of the bar-slip spring components at the perimeter of the joint), shear transfer at the perimeter of the joint occurs through a compression-strut mechanism. Further, it is assumed that this compression-strut mechanism has adequate strength and relatively high stiffness. If, however, concrete cracks at the joint perimeter are open (defined by tensile deformation of the two bar-slip spring components on a joint-beam or joint-column interface), it is assumed that shear transfer occurs through aggregate interlock. The contribution of dowel action is assumed to be negligible, as is indicated by the results of previous

investigations of shear transfer in reinforced concrete elements [Reinhardt and Walraven 1982; Ma et al. 1976].

The results of research by Walraven [1981, 1994] are used as a basis for calibrating the interface shear components of the proposed beam-column joint model. Walraven [1981] develops a model defining the normal and shear stress transferred across a concrete crack surface as a function of slip across the surface and crack width. If cracks are open, this model is used to define the envelope of the force-deformation relationship for the interface-shear components. It is assumed that shear strength as a function of slip across the concrete crack surfaces does not deteriorate at large slip levels. For the case of closed concrete cracks, the interface-shear response is assumed elastic with stiffness defined by the Walraven model for a relatively small crack width opening (0.1 mm). In applying the Walraven model to calibrate the beam-column joint model, it is assumed that the normal stress developed at the concrete crack surface is carried by frame-member longitudinal reinforcement.

Data from an investigation of shear transfer in cracked concrete subjected to cyclic loading [Walraven 1994] and frame member geometry are used to complete calibration of the interface-shear components. As with the shear-panel and bar-slip components of the model, the general hysteretic response model is used to define the response, and model calibration requires definition of the unload-reload response as well as definition of the hysteretic damage rules. Data presented by Walraven show the following characteristics:

- the unloading stiffness is extremely large and does not deteriorate as a function of the load history;
- the reloading stiffness is approximately equal to the initial stiffness; and
- upon reloading, a maximum displacement in excess of the previous maximum displacement is required to develop the same shear strength.

These characteristics are incorporated into the current model by defining an unloading stiffness equal to the initial stiffness predicted for zero slip and a relatively small crack width opening (0.1 mm) and a reloading stiffness equal to the stiffness predicted for zero slip and the current level of crack width opening. Deterioration in strength at a given displacement level under cyclic loading is represented by the reloading-strength degradation model (Eq. 4.4). No deterioration in strength or stiffness is included in the model. The proposed calibration procedure is used to define a shear stress versus slip response history for beam-joint and column-joint

interfaces. Beam and column areas are used to convert these histories to shear force versus slip histories that are appropriate for use in calibrating the interface shear components of the model.

Because the interface shear force is a function both of slip and crack width and because the interface shear component of the joint model is assumed to transfer force in only one direction, implementation of the component model is not as straightforward as for the bar-slip and shear-panel components. The proposed response model explicitly defines shear force as a function of slip and crack width on the interface; thus, it is possible to compute a consistent tangent for the component response and thereby maintain the potential for quadratic convergence of the internal element solution algorithm. However, because the component shear force depends on shear slip and crack opening, the component consistent tangent is not symmetric. This implies that the element tangent also is not symmetric. To maintain symmetry of the element tangent and the potential for quadratic convergence and at the element and structure levels, crack width dependence is defined to be explicit rather than implicit. Thus, at any stage of the solution algorithm, the interface shear force is a function of interface slip and the crack width from the previous converged element solution state.

Figure 4.13 shows interface-shear versus slip response as a function of crack width as predicted using the Walraven [1981] model. These shear force versus slip curves define the envelope to the reversed-cyclic response history. A simulated interface shear stress versus slip response history for a beam-joint interface in a building joint subassemblage subjected to cyclic loading includes the effect of crack width opening; thus, consideration of “cyclic” response for a single crack width opening provides relatively little insight into beam-column joint response.

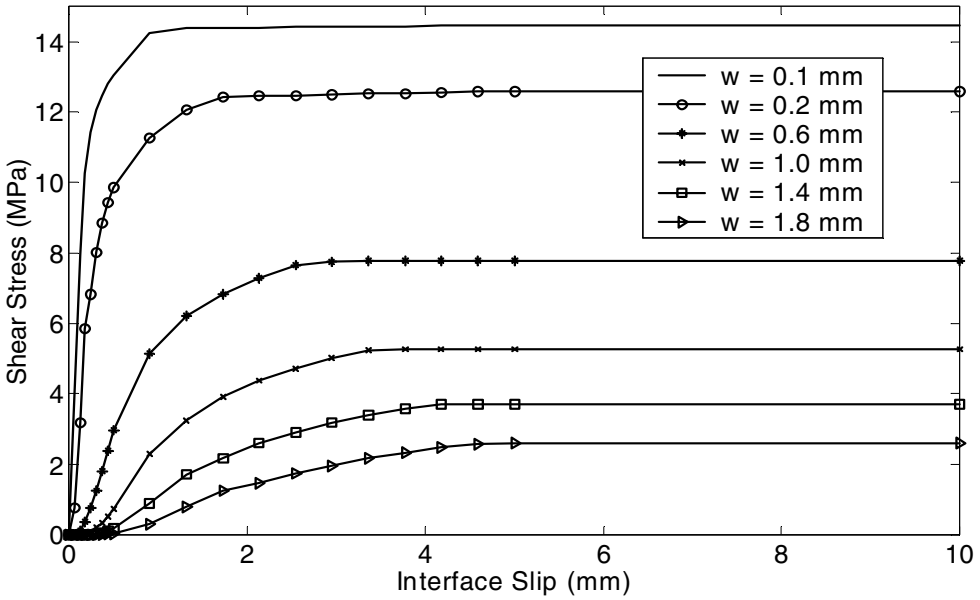

Fig. 4.13. Envelope to shear stress versus slip response history

5 Model Evaluation and Verification

The proposed model and calibration procedures are evaluated through comparison of simulated and observed response for beam-column building subassemblages tested in the laboratory under virtual earthquake loading. Comparison of these data for a series of building beam-column joints investigated by Park and Ruitong [1988] indicates that the proposed model represents the observed failure mechanisms and fundamental response characteristics of these reinforced-concrete building beam-column joints.

Park and Ruitong [1988] tested a series of four building frame subassemblages designed to achieve different levels of ductility under simulated earthquake loading. Figure 5.1 shows an idealization of the building frame subassemblages and the load distribution applied in the laboratory. The beam-column joint of the prototype specimen (Unit 1) was designed in accordance with NZS 3101:1982, design provisions for ductile reinforced concrete frames. The remaining specimens were designed with features that were expected to reduce the ductility capacity. These features included reduced normalized anchorage length for beam bars embedded in the joint (Units 2 and 4) and reduced joint shear capacity to demand ratio (Units 3 and 4). Joint shear capacity was defined, per NZS 3101, by the area of horizontal reinforcement provided as hoops in the joint core and the area of vertical reinforcement provided by column interior longitudinal reinforcement embedded in the joint core. Specimens were subjected to simulated earthquake loading by forcing the column tip through a prescribed pseudo-static reversed-cyclic displacement history. Beam-column joints were subjected to moderate shear demand, with the design joint shear stress less than $0.7\sqrt{f_c}$ MPa with f_c in MPa ($9\sqrt{f_c}$ psi with f_c in psi).

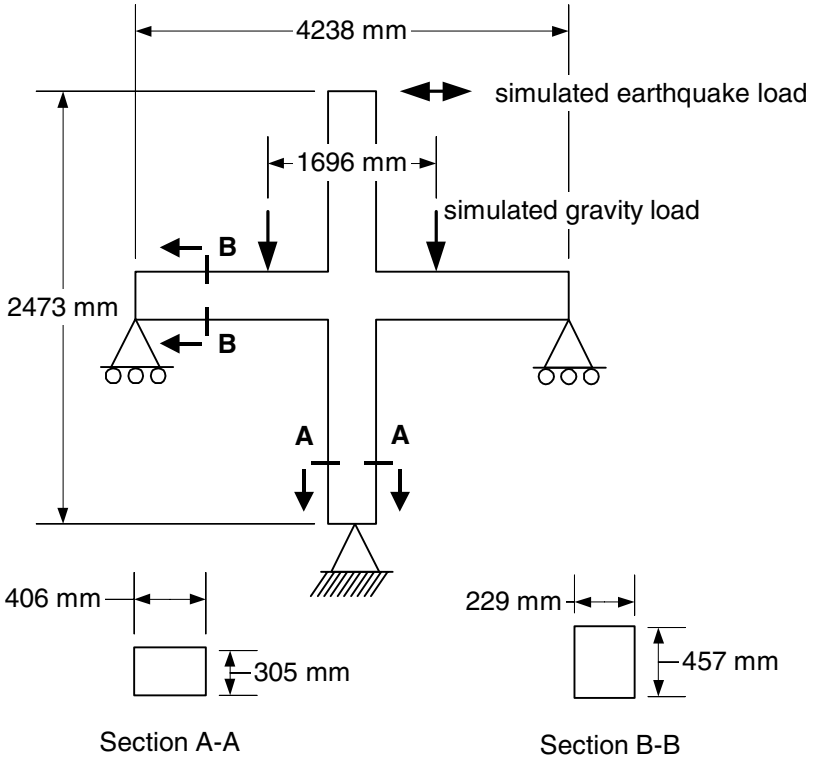

Fig. 5.1. Beam-column building joint subassemblage tested by Park and Ruitong [1988]

Numerical models were developed to simulate the response of the Park and Ruitong subassemblages to laboratory loading. Numerical models comprised lumped-plasticity beam-column elements and the proposed beam-column joint element. Lumped-plasticity beam-column elements were calibrated on the basis of the following assumptions:

1. The elastic flexural stiffness is defined by the cracked section properties.
2. The envelope to the moment-rotation response of the plastic hinge is defined by the computed moment-curvature response of the beam-column cross-section and an assumed plastic-hinge length equal to half the depth of the beam-column element.
3. The hysteretic response of the plastic-hinge is represented by the previously presented general one-dimensional hysteretic response model with load-path parameters defined to represent the observed response of the ductile reinforced concrete flexural elements.

The proposed beam-column joint calibration procedures were employed for the bar-slip and shear-panel components of the model with material, geometric, and design parameters provided by Park and Ruitong. For calibration of the joint shear-panel response, the horizontal

transverse steel ratio was calculated on the basis of the total area of horizontal transverse steel provided in the joint while the vertical transverse steel ratio was calculated on the basis of the total area of the longitudinal steel provided in the column. Since the restraint of the beam-axial deformation provided by the Park and Ruitong test frame is unknown, the interface-shear components are assumed to remain elastic, with stiffness defined on the basis of closed interface cracks.

The proposed beam-column joint model is evaluated through comparison of observed and simulated response for the Park and Ruitong specimens. Figures 5.2 and 5.3 show, respectively, the observed and simulated column tip displacement versus column shear for two of the specimens, Unit 1 and Unit 4. The observed response history for Unit 1 shows significant energy dissipation and no strength loss; for Unit 4, the load-displacement history shows a more pinched response and strength loss at a displacement ductility demand of 5. The observed response histories for Units 2 and 3 are similar with that for Unit 2, exhibiting a significantly pinched load-displacement history as well as strength loss at a ductility demand of 5 and Unit 3 showing moderate pinching of the load-displacement history and minimal strength loss at a ductility demand of 7. The simulated histories exhibit the same fundamental characteristics as the observed histories; though strength loss is delayed until a ductility demand of 7 in the simulated histories.

Tables 5.1 and 5.2 list characteristics of the observed and simulated response histories that are considered in evaluating the model. Comparison of load-displacement histories in Figures 5.2 and 5.3 shows similar response for laboratory and computer models. However, comparison of maximum strength values (Tables 4.2 and 4.3) shows that simulated strength is 8 to 13% less than the observed strength. This discrepancy most likely results from the assumption of a bilinear moment-rotation response envelope for the plastic hinges of the beam-column elements in the computer model. However, this discrepancy could be a function of a too small post-yield stiffness of the shear-panel and bar-slip components of the joint model. If this is the case, this suggests that the proposed model does not represent additional joint stiffness resulting from load-redistribution in the postyield regime.

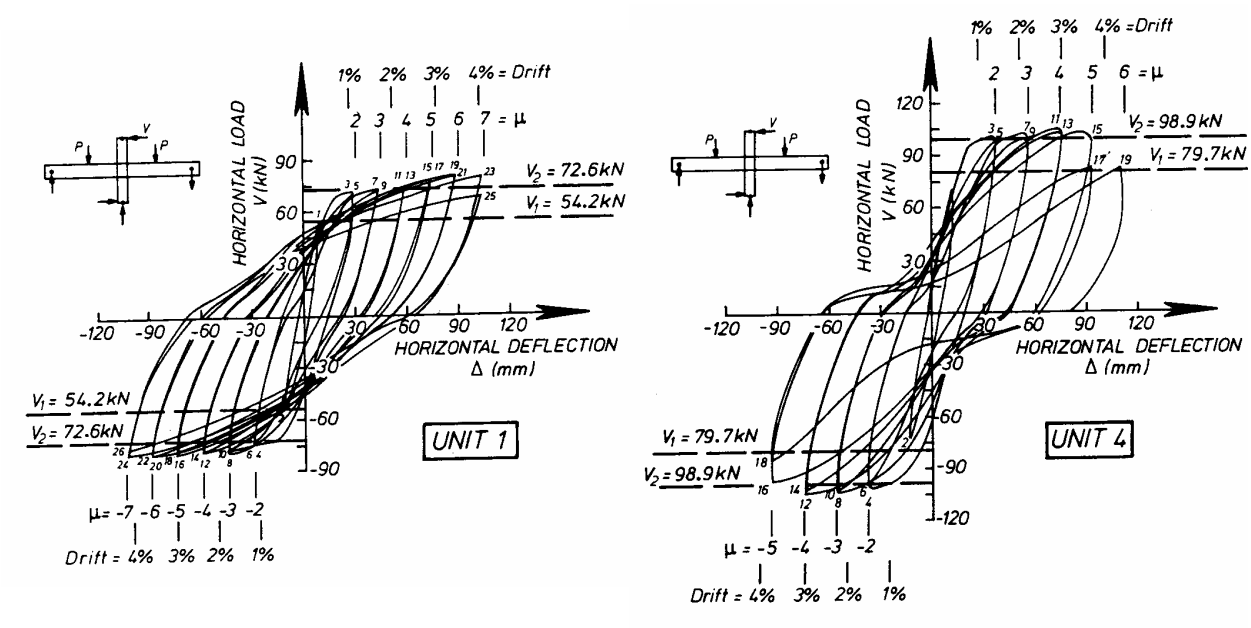

(a) Unit 1 — ductile specimen (b) Unit 4 — limited ductility specimen

Fig. 5.2. Observed response of building subassemblages (Fig. 16, Park and Ruitong [1988])

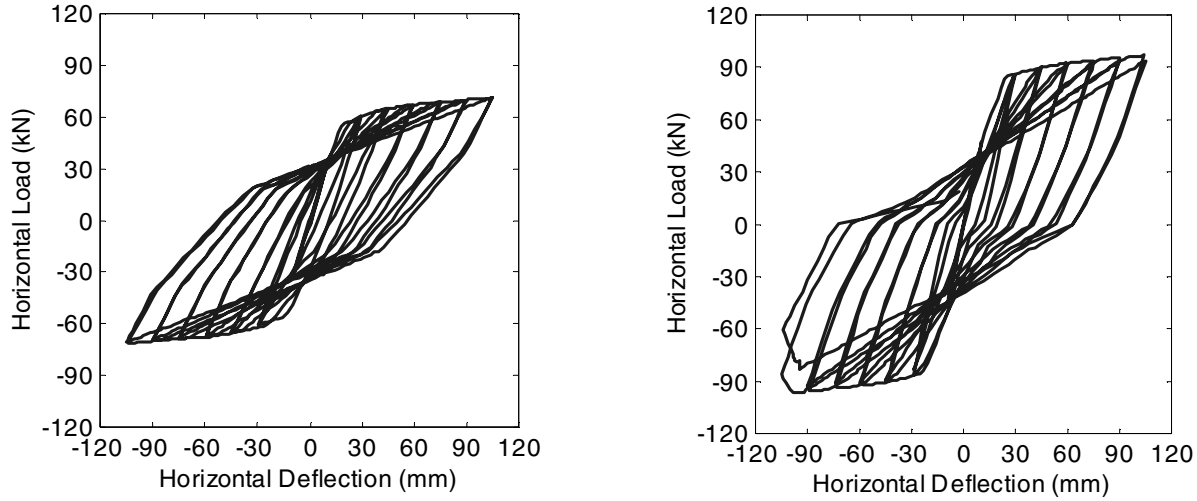

(a) Unit 1 — ductile specimen (b) Unit 4 — limited ductility specimen

Fig. 5.3. Simulated response of the Park and Ruitong [1988] building subassemblages

Table 5.1 Observed response characteristics for Park and Ruitong [1988] specimens

	Unit 1	Unit 2	Unit 3	Unit 4
Maximum strength	80.3 kN	111.7 kN	79.4 kN	106.5 kN
Strength for final load cycle (% of theoretical capacity)	~ 100%	76%	99%	81%
Ductility demand at which substantial strength loss was observed	no substantial loss at $\mu = 7$	$\mu = 5$	no substantial loss at $\mu = 7$	$\mu = 5$
Pinching of hysteresis loops	not significant	significant	More than Unit 1; less than Units 2 & 4	significant
Maximum concrete crack width in the joint.	0.6 mm	0.4 mm	1.4 mm	1.1 mm
Impact of bar slip	Units 1 & 2 have the same joint shear capacity-demand ratio, but Unit 2 has larger beam bars. This appears to have resulted in more inelastic deformation due to bar slip and less due to joint shear deformation for Unit 2 than for Unit1.		Units 3 & 4 have the same joint shear capacity-demand ratio, but Unit 4 has larger beam bars. This appears to have resulted in more inelastic deformation due to bar slip and less due to joint shear deformation for Unit 4 than for Unit 3.	
Contribution of joint deformation to total displacement at high level	9 – 14%	7 - 12%	23 – 38%	15 – 19%

Table 5.2. Simulated response characteristics for Park and Ruitong specimens

	Unit 1	Unit 2	Unit 3	Unit 4
Maximum strength	71.2 kN	96.7 kN	69.8 kN	97.7 kN
Ductility demand at which strength loss is observed	no substantial loss at $\mu = 7$	$\mu = 7$	no substantial loss at $\mu = 7$	$\mu = 7$
Mechanism that controls strength loss		anchorage		anchorage
Pinching of hysteresis loops	not significant	significant	Moderate	significant
Impact of bar slip: Bar slip accounts for what percentage of joint deformation at high-ductility demands	47%	56%	30%	53%
Contribution of joint shear-panel deformation to total deformation at high ductility demands	5 - 6 %	11 – 13%	21 – 23%	14-16%
Contribution of joint deformation to total deformation at high ductility demands	6 – 9%	16 – 24%	21 – 25%	16 – 24%

Comparison of simulated and observed response indicates that the proposed model represents well the observed failure models. The research results provided by Park and Ruitong indicate that failure of beam-bar anchorage likely resulted in strength loss for Units 2 and 4. The proposed model represents this aspect of response with strength deterioration resulting from failure of beam bar-slip slip components rather than the shear-panel component. However, while the model represents the observed failure mechanism, the ductility demand at which strength loss occurs and the rate of strength loss are not represented with a high level of accuracy. The discrepancy in the simulated failure point must be attributed to the simplicity of the model; discrepancy in post-peak response may be attributed to inadequacies in the data used for calibration and may be mitigated in future work. Park and Ruitong propose that for Units 2 and 4, anchorage failure of beam longitudinal reinforcement contributes significantly to global specimen deformation at high ductility demands, with the result that joint deformation is limited. The characteristic of response is represented well by the model with the joint bar-slip mechanism contributing to 56% and 53% of the joint deformation for Units 2 and 4, but only 36% for Unit 3.

Despite the simplicity of the proposed model, evaluation of experimental and numerical data indicates that the model represents joint deformation. Park and Ruitong monitor joint deformation in the laboratory by measuring the deformation along the diagonals of the joint. Instrumentation is mounted in the vicinity of beam and column reinforcement anchorage zones. Thus, measured joint deformation likely includes shear deformation of the joint core as well as some deformation associated with anchorage failure. If the deformation measured by Park and Ruitong is assumed to include only shear distortion of the joint core, then comparison of data in Tables 4.2 and 4.3 indicates that, with the exception of Unit 2, the proposed model underestimates the contribution of joint deformation to global deformation. If the deformation measured by Park and Ruitong is assumed to include shear distortion and anchorage-zone deformation, then comparison of data in Tables 4.2 and 4.3 indicates that, with the exception of Unit 2, the proposed model can be used to simulated observed response.

Comparison of the observed and simulated response of the Park and Ruitong specimens suggests that the proposed model and calibration procedures are appropriate for use in simulating the response of reinforced concrete beam-column joints in building frames. Simulated response histories represent well the fundamental characteristics of observed response including energy dissipation within the joint and beam-column joint failure modes. The proposed model provides a simple representation of the inelastic joint response mechanisms and the proposed calibration

procedures provide a simple, but general, approach to quantifying the response of these mechanism. However, the simplicity and generality of the model appear to limit the accuracy with which load-deformation response, specifically post-yield and post-peak stiffness, are represented.

6 Summary

A model is proposed for use in simulating the inelastic response of typical beam-column joints in two-dimensional nonlinear analysis of reinforced concrete frames. This model represents the mechanisms that may determine inelastic beam-column joint behavior through the combined action of one-dimensional shear-panel, bar-slip and interface-shear components. Constitutive models are developed to define the response of the shear-panel and bar-slip components of the model; these procedures define response on the basis of concrete and steel material properties, the beam-column joint geometry, and the distribution of reinforcing steel design. Comparison of simulated and observed response for a series of beam-column joint building subassemblages indicates that the proposed model represents well the fundamental characteristics of response for joints subjected to moderate shear demands.

REFERENCES

Alath, S. and Kunnath, S. K. (1995). "Modeling Inelastic Shear Deformation in RC Beam-Column Joints *Engineering Mechanics: Proceedings of 10th Conference: University of Colorado at Boulder, Boulder, Colorado, May 21-24, 1995*. Vol. 2. New York: ASCE: 822-825.

ACI Committee 318 (1999). *Building Code Requirements for Structural Concrete (ACI 318-99) and Commentary (ACI 318R-99).* Farmington Hills, Michigan: American Concrete Institute.

Anderson, J.C. and Townsend, W.H. (1977). "Models for RC Frames with Degrading Stiffness," *Journal of the Structural Division, ASCE*. **103** (ST12): 1433-1449.

Bonacci, J.F. and Pantazopoulou, S.J. (1993). "Parametric Investigation of Joint Mechanics." *ACI Structural Journal* **90** (1): 61-71.

Clyde, C., Pantelides, C.P. and Reaveley, L.D. (2000). "Performance-Based Evaluation of Exterior Reinforced Concrete Building Joints for Seismic Excitation." *Pacific Earthquake Engineering Research Report, PEER 2000/05*. Berkeley: University of California.

Durrani, A.J. and Wight, J.K. (1985). "Behavior of Interior Beam-to-Column Connections Under Earthquake-Type Loading." *ACI Structural Journal* **82** (3): 343-350.

EERI (1994). *Northridge Earthquake January 17,1994, Preliminary Reconnaissance Report.* Ed. J.F. Hall. Oakland, CA: EERI.

Eligehausen, R., Popov, E.P. and Bertero, V.V. (1983). "Local Bond Stress-Slip Relationships of Deformed Bars Under Generalized Excitations." *EERC Report 83/23*. Berkeley: University of California.

El-Metwally, S.E. and Chen, W.F. (1988). "Moment-Rotation Modeling of Reinforced Concrete Beam-Column Connections." *ACI Structural Journal* **85** (4): 384-394.

Elmorsi, M., Kianoush, M.R. and Tso, W.K. (2000). "Modeling Bond-Slip Deformations in Reinforced Concrete Beam-Column," *Canadian Journal of Civil Engineering **27**: 490-505*.

Fleury, F., Reynouard, J.M. and Merabet, O. (2000). "Multicomponent Model of Reinforced Concrete Joints for Cyclic Loading," *Journal of Engineering Mechanics ASCE* **126** (8): 804-811.

Hawkins, N.M., Lin, I.J. and Jeang, F.L. (1982). "Local Bond Strength of Concrete for Cyclic Reversed Loadings." *Bond in Concrete.* P. Bartos (editor). Applied Science Publishers Ltd., London: 151-161.

Krawinkler, H. and Popov, E.P. (1982). "Seismic Behavior of Moment Connections and Joints." *Journal of the Structural Division, ASCE* **108** (2): 373-391.

Leon, R.T. (1990). "Shear Strength and Hysteretic Behavior of Interior Beam-Column Joints." *ACI Structural Journal* **87** (1): 3-11.

Lowes, L.N. (1999). "Finite Element Modeling of Reinforced Concrete Beam-Column Bridge Connections." *Dissertation*. University of California, Berkeley.

Lowes, L.N. and Moehle, J.P. (1999). **"**Evaluation and Retrofit of Beam-Column T-Joints in Older Reinforced Concrete Bridge Structures." *ACI Structural Journal* **96** (4): 519-532.

Ma, S.Y.M., Bertero, V.V. and Popov, E.P. (1976). "Experimental and Analytical Studies on the Hysteretic Behavior of Reinforced Concrete Rectangular and T-Beams." *Earthquake Engineering Research Report 76/2*. Berkeley: University of California.

Malvar, L.J. (1992). "Bond Reinforcement Under Controlled Confinement." *ACI Materials Journal* **89** (6): 593-601.

Matthies, H. and Strang, G. (1979). "The Solution of Nonlinear Finite Element Equations," *International Journal for Numerical Methods in Engineering* **14**: 1613-1626.

Mazzoni, S. and Moehle, J.P. (2001). **"**Seismic Response of Beam-Column Joints in Double-Deck Reinforced Concrete Bridge Frames." *ACI Structural Journal* **98** (3): 259-269.

Meinheit, D.F. and Jirsa, J.O. (1977). "The Shear Strength of Reinforced Concrete Beam-Column Joints." *CESRL Report No. 77-1*. Austin: University of Texas.

Otani, S. (1974). "Inelastic Analysis of RC Frame Structures," *Journal of the Structural Division, ASCE.* **100** (ST7): 1433-1449.

Paulay, T., Park, R. and Priestley, M.J.N. (1978). "Reinforced Concrete Beam-Column Joints Under Seismic Actions," *ACI Journal* **75**: 585-593.

Park, R. and Paulay, T. (1975). *Reinforced Concrete Structures*. New York: John Wiley & Sons.

Park, R. and Ruitong, D. (1988). "A Comparison of the Behavior of Reinforced Concrete Beam-Column Joints Designed for Ductility and Limited Ductility." *Bulletin of the New Zealand National Society of Earthquake Engineering* **21** (4): 255-278.

Park, Y.J. and Ang, A.H.S. (1985). "Mechanistic Seismic Damage Model for Reinforced Concrete." *Journal of Structural Engineering ASCE* **111**(4): 722-739.

Reinhardt, H.W. and Walraven, J.C. (1982). "Cracks in Concrete Subject to Shear." *Journal of the Structural Division, ASCE* **108** (ST1): 207-224.

Shima, H., Chou, L.L. and Okamura, H. (1987). "Bond Characteristics in Post-Yield Range of Deformed Bars." *Concrete Library of JSCE* **10**: 113-124.

Stevens N.J., Uzumeri, S.M. and Collins, M.P. (1991). "Reinforced-Concrete Subjected to Reversed-Cyclic Shear – Experiments and Constitutive Model." ACI Structural Journal **88** (2): 135-146

Viawanthanatepa, S., Popov, E.P. and Bertero, V.V. (1979). "Effects of Generalized Loadings on Bond of Reinforcing Bars Embedded in Confined Concrete Blocks." *Report UCB/EERC-79/ 22*. Berkeley: EERC, University of California.

Vecchio, F.J. and Collins, M.P. (1986). "The Modified-Compression Field Theory for Reinforced-Concrete Elements Subjected to Shear." *Journal of the American Concrete Institute* **83** (2): 219-231.

Walker, S.G. (2001). *Seismic Performance of Existing Reinforced Concrete Beam-column Joints*. M.S. Thesis. University of Washington, Seattle.

Walraven, J.C. (1981). "Fundamental Analysis of Aggregate Interlock." *Journal of the Structural Division, ASCE* **107** (ST11): 2245-2270.

Walraven, J.C. (1994). "Rough Cracks Subjected to Earthquake Loading." *Journal of Structural Engineering, ASCE* **120** (5): 1510 –1524.

PEER REPORTS

PEER reports are available from the National Information Service for Earthquake Engineering (NISEE). To order PEER reports, please contact the Pacific Earthquake Engineering Research Center, 1301 South 46th Street, Richmond, California 94804-4698. Tel.: (510) 231-9468; Fax: (510) 231-9461.

PEER 2003/10 *A Beam-Column Joint Model for Simulating the Earthquake Response of Reinforced Concrete Frames.* Laura N. Lowes, Nilanjan Mitra, and Arash Altoontash. February 2004.

PEER 2003/08 *A Technical Framework for Probability-Based Demand and Capacity Factor Design (DCFD) Seismic Formats*. Fatemeh Jalayer and C. Allin Cornell. November 2003.

PEER 2003/06 *Performance of Circular Reinforced Concrete Bridge Columns under Bidirectional Earthquake Loading*. Mahmoud M. Hachem, Stephen A. Mahin, and Jack P. Moehle. February 2003.

PEER 2003/05 *Response Assessment for Building-Specific Loss Estimation.* Eduardo Miranda and Hesammeddin Aslani. September 2003.

PEER 2003/04 *Experimental Assessment of Columns with Short Lap Splices Subjected to Cyclic Loads*. Murat Melek, John W. Wallace, and Joel Conte. April 2003.

PEER 2003/03 *Probabilistic Response Assessment for Building-Specific Loss Estimation.* Eduardo Miranda and Hesameddin Aslani. September 2003.

PEER 2003/02 *Software Framework for Collaborative Development of Nonlinear Dynamic Analysis Program.* Jun Peng and Kincho H. Law. September 2003.

PEER 2003/01 *Shake Table Tests and Analytical Studies on the Gravity Load Collapse of Reinforced Concrete Frames.* Kenneth John Elwood and Jack P. Moehle. November 2003

PEER 2002/24 *Performance of Beam to Column Bridge Joints Subjected to a Large Velocity Pulse.* Natalie Gibson, André Filiatrault, and Scott A. Ashford. April 2002.

PEER 2002/23 *Effects of Large Velocity Pulses on Reinforced Concrete Bridge Columns.* Greg L. Orozco and Scott A. Ashford. April 2002.

PEER 2002/22 *Characterization of Large Velocity Pulses for Laboratory Testing.* Kenneth E. Cox and Scott A. Ashford. April 2002.

PEER 2002/21 *Fourth U.S.-Japan Workshop on Performance-Based Earthquake Engineering Methodology for Reinforced Concrete Building Structures*. December 2002.

PEER 2002/20 *Barriers to Adoption and Implementation of PBEE Innovations.* Peter J. May. August 2002.

PEER 2002/19 *Economic-Engineered Integrated Models for Earthquakes: Socioeconomic Impacts.* Peter Gordon, James E. Moore II, and Harry W. Richardson. July 2002.

PEER 2002/18 *Assessment of Reinforced Concrete Building Exterior Joints with Substandard Details.* Chris P. Pantelides, Jon Hansen, Justin Nadauld, and Lawrence D. Reaveley. May 2002.

PEER 2002/17 *Structural Characterization and Seismic Response Analysis of a Highway Overcrossing Equipped with Elastomeric Bearings and Fluid Dampers: A Case Study.* Nicos Makris and Jian Zhang. November 2002.

PEER 2002/16 *Estimation of Uncertainty in Geotechnical Properties for Performance-Based Earthquake Engineering.* Allen L. Jones, Steven L. Kramer, and Pedro Arduino. December 2002.

PEER 2002/15 *Seismic Behavior of Bridge Columns Subjected to Various Loading Patterns.* Asadollah Esmaeily-Gh. and Yan Xiao. December 2002.

PEER 2002/14 *Inelastic Seismic Response of Extended Pile Shaft Supported Bridge Structures.* T.C. Hutchinson, R.W. Boulanger, Y.H. Chai, and I.M. Idriss. December 2002.

PEER 2002/13 *Probabilistic Models and Fragility Estimates for Bridge Components and Systems.* Paolo Gardoni, Armen Der Kiureghian, and Khalid M. Mosalam. June 2002.

PEER 2002/12 *Effects of Fault Dip and Slip Rake on Near-Source Ground Motions: Why Chi-Chi Was a Relatively Mild M7.6 Earthquake.* Brad T. Aagaard, John F. Hall, and Thomas H. Heaton. December 2002.

PEER 2002/11 *Analytical and Experimental Study of Fiber-Reinforced Strip Isolators*. James M. Kelly and Shakhzod M. Takhirov. September 2002.

PEER 2002/10 *Centrifuge Modeling of Settlement and Lateral Spreading with Comparisons to Numerical Analyses***.** Sivapalan Gajan and Bruce L. Kutter. January 2003.

PEER 2002/09 *Documentation and Analysis of Field Case Histories of Seismic Compression during the 1994 Northridge, California, Earthquake.* Jonathan P. Stewart, Patrick M. Smith, Daniel H. Whang, and Jonathan D. Bray. October 2002.

PEER 2002/08 *Component Testing, Stability Analysis and Characterization of Buckling-Restrained Unbonded Braces™.* Cameron Black, Nicos Makris, and Ian Aiken. September 2002.

PEER 2002/07 *Seismic Performance of Pile-Wharf Connections.* Charles W. Roeder, Robert Graff, Jennifer Soderstrom, and Jun Han Yoo. December 2001.

PEER 2002/06 *The Use of Benefit-Cost Analysis for Evaluation of Performance-Based Earthquake Engineering Decisions*. Richard O. Zerbe and Anthony Falit-Baiamonte. September 2001.

PEER 2002/05 *Guidelines, Specifications, and Seismic Performance Characterization of Nonstructural Building Components and Equipment*. André Filiatrault, Constantin Christopoulos, and Christopher Stearns. September 2001.

PEER 2002/04 *Consortium of Organizations for Strong-Motion Observation Systems and the Pacific Earthquake Engineering Research Center Lifelines Program: Invited Workshop on Archiving and Web Dissemination of Geotechnical Data, 4–5 October 2001*. September 2002.

PEER 2002/03 *Investigation of Sensitivity of Building Loss Estimates to Major Uncertain Variables for the Van Nuys Testbed.* Keith A. Porter, James L. Beck, and Rustem V. Shaikhutdinov. August 2002.

PEER 2002/02 *The Third U.S.-Japan Workshop on Performance-Based Earthquake Engineering Methodology for Reinforced Concrete Building Structures*. July 2002.

PEER 2002/01 *Nonstructural Loss Estimation: The UC Berkeley Case Study. Mary C. Comerio and John C. Stallmeyer.* December 2001.

PEER 2001/16 *Statistics of SDF-System Estimate of Roof Displacement for Pushover Analysis of Buildings.* Anil K. Chopra, Rakesh K. Goel, and Chatpan Chintanapakdee. December 2001.

PEER 2001/15 *Damage to Bridges during the 2001 Nisqually Earthquake.* R. Tyler Ranf, Marc O. Eberhard, and Michael P. Berry. November 2001.

PEER 2001/14 *Rocking Response of Equipment Anchored to a Base Foundation.* Nicos Makris and Cameron J. Black. September 2001.

PEER 2001/13 *Modeling Soil Liquefaction Hazards for Performance-Based Earthquake Engineering.* Steven L. Kramer and Ahmed-W. Elgamal. February 2001.

PEER 2001/12 *Development of Geotechnical Capabilities in OpenSees.* Boris Jeremic. September 2001.

PEER 2001/11 *Analytical and Experimental Study of Fiber-Reinforced Elastomeric Isolators*. James M. Kelly and Shakhzod M. Takhirov. September 2001.

PEER 2001/10 *Amplification Factors for Spectral Acceleration in Active Regions.* Jonathan P. Stewart, Andrew H. Liu, Yoojoong Choi, and Mehmet B. Baturay. December 2001.

PEER 2001/09 *Ground Motion Evaluation Procedures for Performance-Based Design.* Jonathan P. Stewart, Shyh-Jeng Chiou, Jonathan D. Bray, Robert W. Graves, Paul G. Somerville, and Norman A. Abrahamson. September 2001.

PEER 2001/08 *Experimental and Computational Evaluation of Reinforced Concrete Bridge Beam-Column Connections for Seismic Performance*. Clay J. Naito, Jack P. Moehle, and Khalid M. Mosalam. November 2001.

PEER 2001/07 *The Rocking Spectrum and the Shortcomings of Design Guidelines.* Nicos Makris and Dimitrios Konstantinidis. August 2001.

PEER 2001/06 *Development of an Electrical Substation Equipment Performance Database for Evaluation of Equipment Fragilities*. Thalia Agnanos. April 1999.

PEER 2001/05 *Stiffness Analysis of Fiber-Reinforced Elastomeric Isolators.* Hsiang-Chuan Tsai and James M. Kelly. May 2001.

PEER 2001/04 *Organizational and Societal Considerations for Performance-Based Earthquake Engineering.* Peter J. May. April 2001.

PEER 2001/03 *A Modal Pushover Analysis Procedure to Estimate Seismic Demands for Buildings: Theory and Preliminary Evaluation.* Anil K. Chopra and Rakesh K. Goel. January 2001.

PEER 2001/02 *Seismic Response Analysis of Highway Overcrossings Including Soil-Structure Interaction.* Jian Zhang and Nicos Makris. March 2001.

PEER 2001/01 *Experimental Study of Large Seismic Steel Beam-to-Column Connections.* Egor P. Popov and Shakhzod M. Takhirov. November 2000.

PEER 2000/10 *The Second U.S.-Japan Workshop on Performance-Based Earthquake Engineering Methodology for Reinforced Concrete Building Structures.* March 2000.

PEER 2000/09 *Structural Engineering Reconnaissance of the August 17, 1999 Earthquake: Kocaeli (Izmit), Turkey.* Halil Sezen, Kenneth J. Elwood, Andrew S. Whittaker, Khalid Mosalam, John J. Wallace, and John F. Stanton. December 2000.

PEER 2000/08 *Behavior of Reinforced Concrete Bridge Columns Having Varying Aspect Ratios and Varying Lengths of Confinement.* Anthony J. Calderone, Dawn E. Lehman, and Jack P. Moehle. January 2001.

PEER 2000/07 *Cover-Plate and Flange-Plate Reinforced Steel Moment-Resisting Connections.* Taejin Kim, Andrew S. Whittaker, Amir S. Gilani, Vitelmo V. Bertero, and Shakhzod M. Takhirov. September 2000.

PEER 2000/06 *Seismic Evaluation and Analysis of 230-kV Disconnect Switches.* Amir S. J. Gilani, Andrew S. Whittaker, Gregory L. Fenves, Chun-Hao Chen, Henry Ho, and Eric Fujisaki. July 2000.

PEER 2000/05 *Performance-Based Evaluation of Exterior Reinforced Concrete Building Joints for Seismic Excitation.* Chandra Clyde, Chris P. Pantelides, and Lawrence D. Reaveley. July 2000.

PEER 2000/04 *An Evaluation of Seismic Energy Demand: An Attenuation Approach.* Chung-Che Chou and Chia-Ming Uang. July 1999.

PEER 2000/03 *Framing Earthquake Retrofitting Decisions: The Case of Hillside Homes in Los Angeles.* Detlof von Winterfeldt, Nels Roselund, and Alicia Kitsuse. March 2000.

PEER 2000/02 *U.S.-Japan Workshop on the Effects of Near-Field Earthquake Shaking.* Andrew Whittaker, ed. July 2000.

PEER 2000/01 *Further Studies on Seismic Interaction in Interconnected Electrical Substation Equipment.* Armen Der Kiureghian, Kee-Jeung Hong, and Jerome L. Sackman. November 1999.

PEER 1999/14 *Seismic Evaluation and Retrofit of 230-kV Porcelain Transformer Bushings*. Amir S. Gilani, Andrew S. Whittaker, Gregory L. Fenves, and Eric Fujisaki. December 1999.

PEER 1999/13 *Building Vulnerability Studies: Modeling and Evaluation of Tilt-up and Steel Reinforced Concrete Buildings.* John W. Wallace, Jonathan P. Stewart, and Andrew S. Whittaker, editors. December 1999.

PEER 1999/12 *Rehabilitation of Nonductile RC Frame Building Using Encasement Plates and Energy-Dissipating Devices.* Mehrdad Sasani, Vitelmo V. Bertero, James C. Anderson. December 1999.

PEER 1999/11 *Performance Evaluation Database for Concrete Bridge Components and Systems under Simulated Seismic Loads.* Yael D. Hose and Frieder Seible. November 1999.

PEER 1999/10 *U.S.-Japan Workshop on Performance-Based Earthquake Engineering Methodology for Reinforced Concrete Building Structures.* December 1999.

PEER 1999/09 *Performance Improvement of Long Period Building Structures Subjected to Severe Pulse-Type Ground Motions*. James C. Anderson, Vitelmo V. Bertero, and Raul Bertero. October 1999.

PEER 1999/08 *Envelopes for Seismic Response Vectors*. Charles Menun and Armen Der Kiureghian. July 1999.

PEER 1999/07 *Documentation of Strengths and Weaknesses of Current Computer Analysis Methods for Seismic Performance of Reinforced Concrete Members.* William F. Cofer. November 1999.

PEER 1999/06 *Rocking Response and Overturning of Anchored Equipment under Seismic Excitations.* Nicos Makris and Jian Zhang. November 1999.

PEER 1999/05 *Seismic Evaluation of 550 kV Porcelain Transformer Bushings*. Amir S. Gilani, Andrew S. Whittaker, Gregory L. Fenves, and Eric Fujisaki. October 1999.

PEER 1999/04 *Adoption and Enforcement of Earthquake Risk-Reduction Measures.* Peter J. May, Raymond J. Burby, T. Jens Feeley, and Robert Wood.

PEER 1999/03 *Task 3 Characterization of Site Response General Site Categories*. Adrian Rodriguez-Marek, Jonathan D. Bray, and Norman Abrahamson. February 1999.

PEER 1999/02 *Capacity-Demand-Diagram Methods for Estimating Seismic Deformation of Inelastic Structures: SDF Systems*. Anil K. Chopra and Rakesh Goel. April 1999.

PEER 1999/01 *Interaction in Interconnected Electrical Substation Equipment Subjected to Earthquake Ground Motions.* Armen Der Kiureghian, Jerome L. Sackman, and Kee-Jeung Hong. February 1999.

PEER 1998/08 *Behavior and Failure Analysis of a Multiple-Frame Highway Bridge in the 1994 Northridge Earthquake.* Gregory L. Fenves and Michael Ellery. December 1998.

PEER 1998/07 *Empirical Evaluation of Inertial Soil-Structure Interaction Effects.* Jonathan P. Stewart, Raymond B. Seed, and Gregory L. Fenves. November 1998.

PEER 1998/06 *Effect of Damping Mechanisms on the Response of Seismic Isolated Structures.* Nicos Makris and Shih-Po Chang. November 1998.

PEER 1998/05 *Rocking Response and Overturning of Equipment under Horizontal Pulse-Type Motions.* Nicos Makris and Yiannis Roussos. October 1998.

PEER 1998/04 *Pacific Earthquake Engineering Research Invitational Workshop Proceedings, May 14–15, 1998: Defining the Links between Planning, Policy Analysis, Economics and Earthquake Engineering.* Mary Comerio and Peter Gordon. September 1998.

PEER 1998/03 *Repair/Upgrade Procedures for Welded Beam to Column Connections*. James C. Anderson and Xiaojing Duan. May 1998.

PEER 1998/02 *Seismic Evaluation of 196 kV Porcelain Transformer Bushings.* Amir S. Gilani, Juan W. Chavez, Gregory L. Fenves, and Andrew S. Whittaker. May 1998.

PEER 1998/01 *Seismic Performance of Well-Confined Concrete Bridge Columns.* Dawn E. Lehman and Jack P. Moehle. December 2000.